

# Journal Pre-proof

Contourite processes associated with the overflow of Pacific Deep Water within the Luzon Trough: Conceptual and regional implications

Shaoru Yin, F. Javier Hernández-Molina, Richard Hobbs, Jinyao Gao, Weifeng Ding, Chunguo Yang, Lin Lin, Huodai Zhang, Ziyin Wu, Jiabiao Li

PII: S0967-0637(20)30248-X

DOI: <https://doi.org/10.1016/j.dsr.2020.103459>

Reference: DSRI 103459

To appear in: *Deep-Sea Research Part I*

Received Date: 28 August 2020

Revised Date: 11 November 2020

Accepted Date: 14 December 2020



Please cite this article as: Yin, S., Javier Hernández-Molina, F., Hobbs, R., Gao, J., Ding, W., Yang, C., Lin, L., Zhang, H., Wu, Z., Li, J., Contourite processes associated with the overflow of Pacific Deep Water within the Luzon Trough: Conceptual and regional implications, *Deep-Sea Research Part I* (2021), doi: <https://doi.org/10.1016/j.dsr.2020.103459>.

This is a PDF file of an article that has undergone enhancements after acceptance, such as the addition of a cover page and metadata, and formatting for readability, but it is not yet the definitive version of record. This version will undergo additional copyediting, typesetting and review before it is published in its final form, but we are providing this version to give early visibility of the article. Please note that, during the production process, errors may be discovered which could affect the content, and all legal disclaimers that apply to the journal pertain.

© 2020 Published by Elsevier Ltd.

# Contourite processes associated with the overflow of Pacific Deep Water within the Luzon Trough: Conceptual and regional implications

Shaoru Yin <sup>a\*</sup>, F. Javier Hernández-Molina <sup>b</sup>, Richard Hobbs <sup>c</sup>, Jinyao Gao <sup>a</sup>, Weifeng Ding <sup>a</sup>, Chunguo Yang <sup>a</sup>, Lin Lin <sup>d</sup>, Huodai Zhang <sup>d\*</sup>, Ziyin Wu <sup>a</sup>, Jiabiao Li <sup>a</sup>

<sup>a</sup> Key Laboratory of Submarine Geosciences, Second Institute of Oceanography, Ministry of Natural Resources, Hangzhou 310012, China

<sup>b</sup> Department of Earth Sciences, Royal Holloway, University of London, Egham, Surrey, TW20 0EX, United Kingdom

<sup>c</sup> Department of Earth Sciences, Durham University, Science Laboratories, South Road, Durham, DH1 3LE, United Kingdom

<sup>d</sup> Guangzhou Marine Geological Survey, Guangzhou 510075, China

\* Corresponding author: [shaoru2017@outlook.com](mailto:shaoru2017@outlook.com); [z1835514387@126.com](mailto:z1835514387@126.com)

## ABSTRACT

Overflows through oceanic gateways govern the exchange of water masses in the world's ocean basins. These exchanges also involve energy, salinity, nutrients, and carbon. As such, the physical features that control overflow can exert a strong influence on regional and global climate. Here, we present the first description of sedimentary processes generated by the overflow of Pacific Deep Water (OPDW). This mass flows southward at approximately 2000 to 3450 m water depth within the Luzon Trough (gateway) from the Pacific Ocean into the South China Sea. OPDW can be divided into: a) a lower, denser layer (including an associated weak counter-current), which has generated a large contourite depositional system (CDS-1) that includes large erosional (channel and moat), depositional (mounded and plastered drift), and mixed (terrace) contourite features along the trough bottom and walls, and b) an upper mixing layer, which has not generated any significant depositional or erosional contourite features. Where OPDW does not reach the seafloor, it is underlain by bottom water that circulates more sluggishly but has generated a second contourite depositional system (CDS-2) made of a large sheet-like drift. The OPDW flow has generally enhanced since the middle to late Miocene, except in the shallower northernmost corridor. In the deeper main trough, reductions in width and depth of the gateway by Taiwan orogenic events have likely accelerated the overflow. The latest significant enhancing may promote widespread development of contourite depositional systems along the South China Sea's lower continental slope and adjacent deeper areas. This work highlights the importance of gateway-confined overflows in controlling the morphology and sedimentary evolution of adjacent deep marine sedimentary systems. A clear understanding of overflow processes and their products is essential for decoding tectonic control in oceanographic or paleoceanographic processes.

**Keywords:** Overflows, sedimentary processes, contourites, gateways, Luzon Trough, Taiwan orogeny, South China Sea

## 1. Introduction

Bathymetric gateways, which may differ in many geometric aspects (e.g., Drake Passage, Tasmanian Seaway, Strait of Gibraltar) (Kennett, 1982; Knutz, 2008), connect all the world's ocean basins, and conduct the exchange of seawater and associated properties and constituents between oceans and seas (Berggren, 1982; Kennet, 1982; Dummann et al., 2019). In the geological past, gateways controlled paleo-circulation patterns and marine basin connections (e.g., Indian Gateway, Indonesian Gateway). The opening / closing, deepening / shallowing of gateways can influence the sedimentary evolution of basins, global ocean circulation, global carbon cycles, poleward temperature gradients, and the exchange and vertical structure of water masses (and associated sedimentary processes) (Knutz, 2008). In turn, these factors determine the distribution of marine biota as well as their longer term evolutionary trajectories (Berggren, 1982; Ricou, 1995; Zachos, et al., 2001; Sijp et al., 2014; Pérez et al., 2019).

The exchange of seawater (and associated properties and constituents) through gateways occurs primarily as lower high-density overflows, as well as upper waters (e.g., buoyant surface waters) necessary to balance the mass transport by overflows across gateways (Gordon et al., 2004, 2009, 2011; Legg et al., 2009; Hansen et al., 2016; Jochumsen et al., 2017; Sanchez-Leal et al., 2017). Examples of these processes

65 include the deep Nordic overflows through gaps in the Greenland-Iceland-Scotland  
66 ridge and Antarctic Bottom Water overflows from the Weddell and Ross seas in the  
67 Antarctic (Gordon et al., 2004, 2009; Legg et al., 2009), as well as intermediate-depth  
68 overflows from the Red Sea and the Mediterranean (Peters et al., 2005; Legg et al.,  
69 2009; Sanchez-Leal et al., 2017). The history of long-term changes in overflow  
70 behavior could be deduced from the products of overflows, i.e., contourite features.  
71 For example, erosional features represent fast overflows and depositional features  
72 mark relatively weak overflows, where mounded contourites (drifts) indicate faster  
73 currents as compared to sheeted drifts (e.g., Faugères et al., 1999; Hernandez-Molina  
74 et al., 2008; Stow et al., 2009; Rebesco et al., 2014). For many gateways, erosion  
75 represents the most dominant sedimentary process, and high velocity and overflow  
76 currents leave no sedimentary record (Garabato et al., 2002; Gordon et al., 2004, 2009;  
77 Sanchez-Leal et al., 2017). In those gateways with significant sedimentation, the  
78 history of long-term changes in overflows and associated gateway tectonics can be  
79 decoded based on the sedimentary record. In the Faeroe-Shetland gateway, the change  
80 from erosion / non-deposition to enhanced contourite drift accumulation at the early  
81 Pliocene suggests a reduction in meridional overflow transport, which may have been  
82 an important factor for the growth of North Hemisphere ice sheets (Knutz and  
83 Cartwright, 2003). In the Bruce Passage, the development of contourite drifts  
84 recorded the opening and evolution of the gateway (Maldonado et al., 2003;  
85 Hernandez-Molina et al., 2007; Lobo et al., 2011; Garcia et al., 2016). Thus, the rare  
86 sedimentary record and modern seafloor can serve as archives of gateway evolution,



recording the long-term regional tectonic events over time.

At gateway exits, overflows form large-scale contourite features in adjacent ocean basins. These features may be erosional (e.g., channels, furrows), depositional (e.g., drifts, bedforms), or mixed (e.g., terraces) (see McCave et al., 1980; Llave et al., 2007; Garcia et al., 2009; Stow et al., 2013; Hernandez-Molina et al., 2014, 2016; Rebesco et al., 2014; de Weger et al., 2020). Exit features are fairly well documented. By contrast, overflow processes within gateways have not been systematically described. One exception is a general report on overflow of Weddell Sea Deep Water through the Bruce Passage from the Weddell Sea into the Scotia Sea (Hernandez-Molina et al., 2007; Lobo et al., 2011; Garcia et al., 2016).

Pacific Deep Water (PDW), also called North Pacific Deep Water in the north Pacific, overflows from the Pacific Ocean into the Luzon Trough in the Luzon Strait (Fig. 1) through the narrow Bashi Channel and Taitung Canyon (Qu et al., 2006; Zhao et al., 2014, 2016; Zhou et al., 2014, 2018), and then enters the South China Sea through two gaps (Ye et al., 2019) in the Heng-Chun Ridge (Fig. 1A). The overflow of Pacific Deep Water (OPDW), after crossing the Luzon Trough, may gradually get mixed due to energetic internal waves/tides and eddies (Qu et al., 2006; Tian et al., 2006; Zhu et al., 2019), and eventually exits the South China Sea in the intermediate layer through the Luzon Strait (Qu et al., 2000; Tian et al., 2006) and in the upper layer mainly through the Karimata and Mindoro Straits (Qu et al., 2009; Yaremchuk et al., 2009). The narrow trough gateway, the only deep passage connecting the Pacific Ocean and the South China Sea, formed due to the Taiwan orogeny (Huang et al.,

2018). The Luzon Trough is therefore ideal for studying overflow within a confined setting, and the role of tectonics in trough and overflow evolution. In this study, the deep north and narrow middle areas of the Luzon Trough are analyzed in order to: 1) identify primary contourite features within the Luzon Trough, 2) decode the role of OPDW in the formation of these features, 3) investigate the influence of the Taiwan orogeny on the overflow variations, and 4) explore the possible effect of the overflow along the adjacent South China Sea margin.

## **2. Geological and oceanographic setting**

### *2.1 Geological background of the Luzon Strait*

The South China Sea (Fig. 1A) formed during the Oligocene to middle Miocene (Taylor and Hayes, 1980; Li et al., 2014) with eastward subduction of the lithosphere along the Manila Trench due to northwest movement of the Philippine Sea plate at a rate of 5–8 cm/year (Hayes and Lewis, 1984; Hall, 2002; Clift et al., 2003; Sibuet and Hsu, 2004). Subduction continued in the middle to late Miocene, with oblique collision between the N-S trending Luzon volcanic arc and the NE-SW trending northern South China margin. The oblique collision initially occurred north of Taiwan at 12–6.5 Ma, then gradually propagated southward (Suppe, 1981; Huang et al., 2018; Clift et al., 2008; Chen et al., 2019). The arc-continent collision is an event referred to as the Taiwan orogeny (Huang et al., 2018). Our study area—the northern and middle Luzon Trough— occupies the Luzon Strait between the South China Sea and the

Pacific Ocean (Fig. 1A). The trough represents a forearc basin bound by an accretionary wedge (Heng-chun Ridge) to the west and a volcanic arc (Luzon Arc) to the east. The formation of this trough began in the middle to late Miocene due to the Taiwan orogeny (Clift et al., 2008; Huang et al., 2018).

## 2.2 Oceanographic setting of the Luzon Strait

The Luzon Strait hosts a distinctive inflow-outflow-inflow structure in vertical (Fig. 1B) (Review in Zhu et al., 2019; Cai et al., 2020). In the upper layer, the North Pacific Tropical Water (NPTW), with a density of  $1024 \text{ kg/m}^3$  (Qu et al., 1999), flows into the South China Sea and contributes to forming the South China Sea Surface Water (SSW) between 0 and 500 m water depth, with a density between 1021.0 and  $1026.8 \text{ kg/m}^3$  (Qu et al., 2006; Tian et al., 2006; Zhang et al., 2015; Cai et al., 2020). The upper layer inflow is induced by the Kuroshio Current intrusion (Review in Cai et al., 2020). In the middle layer, the South China Sea Intermediate Water (SIW, a density between  $1026.8$  and  $1027.6 \text{ kg/m}^3$ ) flows out of the South China Sea into the Pacific Ocean and contributes to circulation of the North Pacific Intermediate Water (NPIW, a density of  $1026.5$  to  $1027.6 \text{ kg/m}^3$ ) between ~500 and ~1500 m water depth (Qu et al., 1999; Tian et al., 2006; Cai et al., 2020). In the deep layer, the PDW, with a potential density of  $1036.7 \text{ kg/m}^3$  (referenced to 2000 decibar) to  $1045.8 \text{ kg/m}^3$  (referenced to 4000 decibar) (Kaneko et al., 2001), flows into the South China Sea as a dense overflow (OPDW) between ~1500 and 2450 m water depth and forms the South China Sea Deep Water (SDW) with a potential density (referenced to 2000

decibar) of 1036.7 to 1036.8 kg/m<sup>3</sup>, and Bottom water (SBW) with a potential density (referenced to 2000 decibar) larger than 1036.8 kg/m<sup>3</sup> (Qu et al., 2006; Zhao et al., 2014; Zhou et al., 2018; Ye et al., 2019). The deep layer inflow and middle layer outflow are driven by baroclinic pressure gradient across the Luzon Strait induced by the density differences between the South China Sea basin and the Pacific Ocean (Fig. 1C. Review in Zhu et al., 2019).

The OPDW, which occurs at depths below ~2000 m with a potential density (referenced to 2000 decibar) of 1036.8 to 1036.9 kg/m<sup>3</sup> (Zhao et al., 2014; Zhou et al., 2018), enters the Luzon Strait (Fig. 1) primarily through the Bashi Channel (1.2 Sv, where 1 Sv = 1×10<sup>6</sup> m<sup>3</sup>/s) and secondarily through Taitung Canyon (0.4 Sv) (Zhao et al., 2014). The overflow then flows southward along the northern Luzon Trough through the narrow, middle part into the southern trough, to finally enter the South China Sea (Fig. 1). This final stage primarily occurs through two gaps (0.73 and 0.45 Sv) in the Heng-Chun Ridge (Zhao et al., 2014). The velocity of the present-day overflow within the Luzon Trough can reach up to 30 cm/s (Zhao et al., 2014, 2016; Zhou et al., 2014). The OPDW exhibits significant seasonal and intraseasonal variations (Zhou et al., 2014; Zhao et al., 2016), including intensified, thicker, deeper, denser flows with higher transports in late fall (October–December) and weakened, thinner, shallower, lighter flows with lower transports in spring (March–May). This overflow is driven by a persistent baroclinic pressure gradient between the Pacific Ocean and the South China Sea due to strong diapycnal mixing in the Sea (Qu et al., 2006; Tian et al., 2009; Zhou et al., 2018), which is induced by energetic internal tides,

internal waves, and mesoscale eddies (Review in Zhu et al., 2019).

### 3. Materials and methods

This study used multibeam swath bathymetry, multichannel seismic reflection profiles, surface samples, and oceanographic data.

#### 3.1 Multibeam swath bathymetric surveys

The bathymetric survey, which covered the entire Luzon Trough (Fig. 1A), was conducted by the Xiangyanghong 14 vessel during the Luzon Strait cruise, from 23 December 2005 to 4 January 2006, using a RESON SeaBat 8150 multibeam system. The original multibeam sounding data were processed using Caris HIPS and SIPS software (version 8.1.9). The final high-resolution seabed digital terrain model was built at a 100 m grid resolution using the swath angle surface method of Caris HIPS and SIPS software (Fig. 2).

The bathymetric data are used to identify modern contourite features together with seismic data following the morphological and seismic criteria defined by Fauguères et al. (1999), Rebesco and Stow (2001), Rebesco (2005), Nielsen et al., (2008), Rebesco and Camerlenghi (2008), and Rebesco et al. (2014).

#### 3.2 Seismic reflection data

Fourteen multichannel 2D seismic reflection profiles (Fig. 1A) spanning a total

length of ~1200 km were collected on five cruises between 1995 and 2009. These included the R/V Maurice Ewing survey EW9509 (Schnuerle et al., 2008) from 23 August 1995 to 24 September 1995; the R/V Marcus G. Langseth expeditions MGL0905 (McIntosh et al., 2013a) from 1 April 2009 to 29 April 2009; MGL0906 (McIntosh et al., 2013b) from 4 May 2009 to 4 June 2009 and MGL0908 (McIntosh et al., 2014) from 16 June 2009 to 25 July, 2009; and the Malina Trench Cruise of the Xiangyanghong 10 vessel in July 2016. The seismic data have a dominant frequency range between 30 and 60 Hz, giving a vertical resolution (tuning thickness) of  $v/240$  to  $v/120$  ( $v$  represents average interval velocity). Average interval velocity was estimated at about 1600 m/s from the average p-wave velocity for sediment 434 m thick at IODP 349 site U1431 (Fig. 1A. Expedition Scientists, 2014), along the abyssal plain of the South China Sea, near the study area. The other four sites (IODP 349 U1432 through U1435) were not used for average interval velocity estimation because their measured p-wave velocities were of poor quality and/or incomplete, or influenced by very high carbonate content. The average interval velocity (1600 m/s) was used to estimate sedimentary thickness and perform a time-depth conversion below the modern seafloor in the Luzon Trough. Seismic data were processed using a standard pre-stack time-migration procedure. Major processing steps included denoising, deconvolution, amplitude correction, trace selection, velocity analysis and model building, and time migration.

The seismic data were used to identify large subsurface contourite features within the Luzon Trough and also to show water mass structure at the profile sites.

The seismic stratigraphic analysis was performed following the conventional method and basic criteria proposed by Mitchum et al. (1977) and Catuneanu et al. (2009). This method uses reflection terminations to identify discontinuities and internal reflection configurations, and unit shapes to characterize seismic facies. The lack of wells in the Luzon Trough impedes good age control of the seismic units. Thus, the age of the sediment base in the Luzon Trough was inferred from the tectonic background, i.e., Taiwan orogeny (e.g., Suppe, 1981; Teng, 1990; Lee et al., 1993; Lin et al., 2002; Yang et al., 2014), and was referenced to stratigraphic interpretations for the northern Luzon Trough by Huang et al. (2018).

### *3.3 Surface sediment samples*

Four box surface sediment samples, GX118BC, GX128BC, GX133BC, and GX138BC, were collected in the northern Luzon Trough (Fig. 1A). The grain size of these samples was measured using a Mastersizer 2000 laser diffraction particle size analyzer. These samples were used to determine dominant sedimentary facies of the seafloor within the modern trough and to assist in the comprehensive identification of contourites by bathymetric and seismic data.

### *3.4 Oceanographic data*

Regional oceanographic data, including salinity and temperature, were provided by the NOAA World Ocean Database 2013

(<https://www.nodc.noaa.gov/OC5/WOD13/data13geo.html>). These data show the characteristics of water masses in the South China Sea, northwest Pacific Ocean, and within the Luzon Trough (Fig. 1B). Data were also used to link the regional water masses to present-day, large contourite features within and adjacent to the Luzon Trough.

### 3.5 Nomenclature

For simplicity, we use the term contourites to refer to sediments deposited or substantially reworked by the persistent action of bottom currents, which could also be related to large-scale bedforms, i.e., sediment waves. This term therefore includes a variety of sediments affected by different types of currents (Rebesco et al., 2014). Thick, extensive sedimentary accumulations are referred to as contourite drifts (Faugères et al., 1999).

## 4. Results

### 4.1 General morphology of the Luzon Trough

The Luzon Trough extends southward from Taiwan Island along about 650 km to Luzon Island (Figs. 1A and 2). Averaging 50 km in width, the trough typically assumes a U-shape in cross-section with a relatively smooth bottom, steep sides and gradients of 3° to 25°. The Heng-chun Ridge to the west (Fig. 1A) is characterized by linear accretionary ridges that parallel the Luzon Trough. A number of sub-circular



depressions are also present to the west, mainly along the Heng-chun Ridge at water depths between 3000 and 3500 m. These depressions range from 8 to 18 km in length, 2.5 to 10 km in width, and 200 to 450 m in depth (Fig. 2B). The Luzon volcanic arc, east of the Luzon Trough (Fig. 1A), includes more than a dozen connected seamounts at water depths between 2500 and 3000 m. These reach heights of 650 to 2600 m.

The Luzon Trough itself consists of three primary trough areas. The northern trough trends N-S, whereas the middle and southern troughs trend NE-SW (Figs. 1 and 2). The northern trough reaches a width of 65 km and bottom depths of 2600 to 3700 m. Its north end connects to two narrower and shallower northeast-trending corridors respectively referred to as C-1 and the Bashi Channel. The middle trough is a narrow, short passage, 7–10 km wide and 20 km long, with bottom depths of 3200 to 3650 m. The southern trough is up to 40 km wide and has bottom depths of 2800 to 3400 m. The whole trough has two main gaps along its western side. Referred to as Outlet-1 and Outlet-2 (Fig. 2), these gaps reside at ~2850 m water depth and connect the southern trough to the South China Sea.

A sill, herein referred to as the Bashi sill, transects the head of the Bashi Channel (Figs. 1 and 2). The sill runs 25 km in length, spans 5 km in width, and resides at water depths of 2050 to 2450 m. Three large isolated bathymetric highs (E1, E2, and E3) reach heights of 200 to 1000 m and are spaced roughly equidistant along the floor of the Bashi Channel and the southern trough (Fig. 2). They form oval to linear features in plan view, with long axes of 8 to 9 km and short axes of 4 to 5 km.

## 4.2 General seismic stratigraphic framework

Three main seismic units (SUs) were identified in the northern and middle areas of the Luzon Trough (Figs. 4–7). These units (SU3 to SU1, from bottom to top) are bound by an acoustic basement beneath SU3, two internal regional discontinuities (H2 and H1, from bottom to top), and the modern seafloor at the top of SU1.

The acoustic basement, which is characterized by reflection-free or discontinuous reflection areas, lies exposed or is locally overlain by thin sediment along the trough wall. Within the trough bottom, seismic unit SU3 overlies the basement. SU3 exhibits moderately continuous, variable-amplitude reflections that show a divergent basin-fill configuration. A reverse fault cuts through the SU3 in the northern trough (Figs. 4 and 5).

The H2 discontinuity defines the top of seismic unit SU3 and the base of seismic unit SU2. This surface appears as continuous, high-amplitude reflections with occasional partial erosional truncation over the underlying seismic unit SU3. SU2 generally shows continuous, high-amplitude reflections that form a sheeted to mounded or wedge-like shape with an aggradational internal configuration (Figs. 4–7). The lower part of SU2 contains a chaotic to semi-transparent reflection package that appears on six of seven examined seismic lines within the main axis of the trough. Similar deposits appear locally in SU1 and on the trough walls.

The H1 discontinuity defines the top of seismic unit SU2 and the base of seismic unit SU1. This surface is characterized by a continuous, high-amplitude reflection.

The upper boundary of SU1 is the modern seafloor. SU1 exhibits moderate- to high-amplitude reflections that show an aggradational internal configuration. The unit exhibits a mounded external form within the C-1 corridor of the northern trough and also within the southern trough (Figs. 4, 5, and 7). Within the main axis of the northern trough (Fig. 6), this unit is generally sheeted rather than mounded, yet it may be mounded locally.

#### *4.3 Gateway contourite features: morphosedimentary and seismic characteristics*

All along the length of the north and middle Luzon Trough, depositional, erosional, and mixed (depositional + erosional) contourite features appear by the trough bottom and walls, even in sections where downslope gravitational features predominate (Fig. 2). Table-I lists the general morphologic parameters of these contourite features.

##### *4.3.1 Depositional features*

Sediment drifts are among the depositional features identified in bathymetric and seismic data. The north and middle parts of the Luzon Trough include mounded, plastered, and sheeted drifts (Fig. 2).

##### *Mounded drifts*

Seven mounded drifts, numbered MD-1 through MD-7, occur along the bottom of the northern and middle troughs (Fig. 2). As implied by their designation, each exhibits a mounded shape. The distribution of erosional and depositional features

indicates that some of the drifts connect laterally, as do MD-1 and MD-2 (Fig. 4), and MD-3 and MD-4 (Fig. 5). The MD-1 drift extends along the western side of corridor C-1 within the northern trough (Figs. 2, 3A, and 4). This drift (Table-I) reaches thicknesses of up to 520 m and gradually thins eastward. MD-1 is characterized by continuous reflections with an aggradational pattern developed primarily within SU2 and SU1 (Fig. 4). SU2 shows a more clearly pronounced mounded morphology than SU1 (Fig. 4).

The MD-2 mounded drift, located just east of MD-1, extends along the eastern side of corridor C-1 (Figs. 2 and 3) and gradually thins westward (Fig. 4). MD-2 (Table-I) reaches thicknesses of up to 320 m and is composed of continuous reflections with an aggradational pattern primarily developed in SU1 and SU2 (Fig. 4).

The nearby MD-3 (up to 190 m thick) and MD-4 drifts (up to 160 m thick) mainly trend NW-SE along the eastern side of a wider section of the C-1 corridor (Figs. 2 and 3A). Both of these drifts show aggradational internal configurations developed within SU1 and SU2 (Fig. 5). Features within SU2 exhibit more mounded morphology than those within SU1. SU3 shows no significant seismic evidence of contourite drifts.

MD-5 and MD-6 occur along the eastern edge of the northern trough bottom (Fig. 2). The mounded shapes here are very smooth (i.e., lower relief). The internal configuration of the drifts is aggradational with continuous, weak to moderate amplitude reflections (Fig. 6). Both of these mounded drifts, up to 130 m thick, occur

only in the uppermost seismic unit, SU1.

MD-7 occurs along the middle trough bottom just north of the E2 bathymetric high (Figs. 2, 3D, and 7). Mainly within SU1 and SU2, high-amplitude reflections outline a mounded, aggradational configuration (Fig. 7). The mounds exhibit higher relief in SU1 than in SU2. The amplitude of the reflection associated with the modern seafloor is higher in western parts of the study area than in eastern parts (Fig. 7).

#### *Plastered drifts*

Plastered drifts are generally smaller and more subtle than mounded drifts (Rebesco et al., 2014). They are often too small to appear in bathymetric data. Seismic profiles exhibit three plastered drifts, PD-1 through PD-3, along the northern and middle Luzon Trough walls (Figs. 6 and 7). PD-1 occurs along the eastern wall of the northern trough and shows a lightly mounded shape (Fig. 6). Up to 40 m thick, PD-1 shows an aggradational internal configuration of continuous reflections having moderate amplitudes (Fig. 6).

PD-2 extends along the western wall of the middle trough, near MD-7 (Fig. 7). Up to 30 m thick, this drift exhibits a smooth, mounded shape and continuous, moderate amplitude reflections indicating an aggradational configuration (Fig. 7). PD-3 occurs along the eastern wall of the middle trough, opposite PD-2 (Fig. 7). Up to 60 m thick, this drift exhibits a smooth, mounded shape and continuous, moderate amplitude reflections indicating upslope progradation (Fig. 7).

#### *Sheeted drifts*

Sheeted drifts are characterized by a broad, very slightly mounded geometry that thins slightly toward the margins (Rebesco et al., 2014). In the Luzon Trough, a single sheeted drift —SD-1, which appears primarily in seismic profiles— extends along the trough bottom below 3500 m water depth (Figs. 2 and 6). Up to 800 m thick, this massive sheeted drift covers the northern trough and a small portion of the southern trough, but occurs only in SU1 and SU2 (Fig. 6). Continuous moderate- to high-amplitude parallel reflections outline an aggradational internal configuration (Fig. 6). Some truncations occur below the modern seafloor along the western edge of the trough bottom. Fine silts cover the surface of the sheeted drift (Fig. 8). Four surface samples (Fig. 2) in the northern trough bottom show fine silt deposits on the seafloor of the sheeted drift (Fig. 8). These samples, GX118BC, GX128BC, GX133BC and GX138BC, respectively gave median grain sizes of 6.69, 6.72, 6.97 and 6.96 phi, all of which mark fine silt.

#### 4.3.2 Erosional features

Two types of erosional features —contourite channels and moats— appear in the bathymetric and seismic data from the northern and middle Luzon Trough.

##### *Contourite channels*

Two contourite channels, CC-1 and CC-2, extend along the northeast-trending C-1 and Bashi Channel of the northern trough (Fig. 2). The CC-1 channel extends southward along the C-1 corridor into the main axis of the northern trough (Fig. 2).

This channel is interrupted by the four mounded drifts, MD-1 through MD-4 (Fig. 2). CC-1 exhibits a V- to U-shape in cross-section and reaches an incisional depth of about 600 m (Fig. 5). Only a limited amount of sediment (sometimes no sediment at all) is found within the CC-1 channel. When present, deposits primarily appear as chaotic, high-amplitude reflections (Fig. 5).

The CC-2 extends southwestward from Bashi Sill (2100 to 2450 m water depth) at the head of Bashi Channel, entering the main course of the northern trough (Fig. 2). This channel exhibits a U-shaped cross-section and reaches an incisional depth of 750 m (Fig. 9). The channel floor is an erosional surface that locally truncates layers of underlying sediment. Some sporadic sedimentary deposits appear within the channel as chaotic to contorted, moderate- to high-amplitude reflections (Fig. 9).

### *Moats*

Moats are a type of valley associated with the mounded drifts identified in SU2 and SU1. Moats within the Luzon Trough are found within two ranges of water depth: 2700 to 3400 m, and 3400 to 3700 m. The moats within the shallower depth range run along the western edges of mounded drifts, MD-1 and MD-3, along the eastern edges of MD-2 and MD-4, and along both edges of MD-7 (Figs. 2, 3, 4, 5, and 7). These moats reach incisional depths of up to 180 m. Moats are commonly wider and deeper along the western sides of the drifts than along the eastern sides (Figs. 4, 5, and 7). Moats within the deeper water depth range run along the eastern sides of the very smooth mounded drifts, MD-5 and MD-6. These moats occur within the northern trough at depths of up to 40 m (Fig. 6). Seismically, all the moat infill appears as

moderate- to high-amplitude layered reflections (Figs. 4–7).

### *4.3.3 Mixed features*

#### *Terraces*

Contourite terraces appear as broad, low-gradient, along-slope features that dip slightly seaward. They develop from mixed (erosional + depositional) bottom-current processes (Rebesco et al., 2014). Within the Luzon Trough, two terraces, T-1 and T-2, extend along the western wall of the northern and middle troughs, respectively (Fig. 2). Terrace T-1 (Table-I), about 600 m thick, exhibits continuous parallel, low-amplitude reflections that outline an internal aggradational configuration (Fig. 6). Terrace T-2 (Table-I) occurs south of terrace T-1 at a similar water depth. Because the seismic survey did not extend to this feature, its internal configuration remains unknown.

## **5. Discussion**

Contourite features in the Luzon Trough have not been reported in the literature to date, but turbidites have been previously described (Huang et al., 2018). We shall first discuss evidence of contourites in the trough and the possible reason why contourites were not easily found in the adjacent onshore outcrops. After that, the sedimentary processes related to these contourites are discussed, as well as the conceptual and regional implications of the sedimentary processes.



### 5.1 Identification of contourite features in the Luzon Trough

The identification and interpretation of contourite features in the Luzon Trough relied on the three-scale approach suggested by Nielsen et al., (2008) and Stow and Smillie (2020). The large-scale (oceanographic setting), middle-scale (seismic architecture), and small-scale (seismic facies, lithology, bedforms) framing allows for consistent interpretation of local- to regional-scale implications.

a) *The oceanographic setting.* The Luzon Trough is the only deep passage connecting the Pacific Ocean and the South China Sea (Qu et al., 2006; Zhao et al., 2014, 2016; Zhou et al., 2014, 2018; Ye et al., 2019). This passage experiences vigorous bottom currents with velocities up to 30 cm/s (Figs. 7B and 9B. Zhao et al., 2014). Such conditions can form depositional or erosional contourite features (Faugères et al. 1999; Stow et al., 2009; Rebesco et al., 2014).

b) *The seismic architecture.* Seismic architecture with regional bathymetric data can detect contourite features (e.g., Faugères et al., 1999; Rebesco and Stow, 2001; Rebesco, 2005; Rebesco and Camerlenghi, 2008; Rebesco et al., 2014). Together with morphological criteria, the mounded drifts (MD-1, MD-2, MD-3, MD-4, MD-5, and MD-6), sheeted drifts (SD-1), and plastered drifts (PD-1, PD-2, and PD-3) (Figs. 3–7) were identified and interpreted based on their regional distributions.

c) *The small scale.* Local seismic facies are also essential for detecting and

452 interpreting bottom current features (Faugères et al., 1999; Nielsen et al., 2008).

453 They include bedforms and seafloor sedimentary facies that may elucidate

454 erosional, depositional, and mixed bottom current features. Physical samples of

455 seafloor material from the sheeted drift SD-1 (Fig. 8) exhibit fine silt deposits

456 with well selected grain size distributions ranging from 6.69 and 6.97 phi. These

457 parameters, characteristic of fine grained contourites (Rebesco et al., 2014;

458 Brackendridge et al., 2018), indicate a low-energy setting swept by a

459 semi-continuous current (Stow et al., 2009; Rebesco et al., 2014).

460 Huang et al. (2018) reported turbidites within Taiwan outcrops north of the Luzon

461 Trough. This report describes contourite features absent from adjacent onshore

462 outcrops that record deep-water sedimentary systems. Contourites do not appear

463 onshore probably because the overflow of Pacific Deep Water (OPDW) only flowed

464 within a narrow trough of an otherwise expansive subduction-collision system.

465 Deformation most likely subjects depocenters to compression and deformation, thus

466 obscuring their morphology and continuity with onshore outcrop expression. Secondly,

467 older ancient sediment exposed onshore could be in a setting with absent or weak

468 OPDW circulation that did not affect these units. Finally, younger, exposed sediments

469 may reflect environments shallower than 2000 m water depth due to a more protracted

470 period of uplift in the north relative to south (Huang et al., 2018), and therefore would

471 not record deeper OPDW activity.

472

## 5.2 Overflow processes and their association with contourite features

### 5.2.1 Contourite depositional systems and gateway water masses

Depositional (drift) and erosional (channel and moat) contourite features described here can be grouped into two contourite depositional systems (CDSs) according to their water depth ranges (2100 to 3400 m, and 3500 to 3700 m water depth). These depth ranges capture contrasting distribution and morphological reliefs of contourite features, which in turn are related to the influences of different water masses.

#### *Contourite depositional system 1 (CDS-1)*

CDS-1 developed at shallower water depths. It includes mounded drifts MD-1 (2780–2850 m water depth), MD-2 (2750–2800 m water depth), MD-3 (2600–2670 m water depth), MD-4 (2590–2630 m water depth), and MD-7 (3200–3400 m water depth) as well as their associated moats. All three plastered drifts, PD-1 (2500–2800 m water depth), PD-2 (2900–3200 m water depth), and PD-3 (3000–3200 m water depth) also occur in CDS-1. It furthermore includes both contourite channels, CC-1 (2600–3000 m water depth) and CC-2 (2650–2700 m). Except for MD-7, PD-2, and PD-3, which occur in the middle trough, most of these features occur in the northern trough. This depositional system overlaps with the OPDW depth range (2000 to 3450 m water depth), which is characterized by high current velocity (Figs. 10 and 11, Zhao et al., 2014), low temperature, and high salinity (Fig. 12) within the trough.

The fact that larger-scale moats occur only along the western sides of the mounded

drifts indicates that these features were formed by a southward-flowing geostrophic flow concentrated along the western side of the Luzon Trough (right side of the flow) due to the influence of the Coriolis force. This interpretation is consistent with the southward current direction and the geostrophic character of the OPDW reported by a number of authors (Qu et al., 2006; Zhao et al., 2014, 2016; Zhou et al., 2014; Ye et al., 2019). The interpretation is also consistent with the westward deviation of the dense OPDW documented by salinity and temperature profiles across the trough (Fig. 12). The OPDW velocity of up to 16 cm/s in the main trough (Fig. 7) (Zhao et al., 2014) resembles current velocities observed in other areas with similar types of drifts and moats along the Atlantic and Antarctic margins (Faugères et al., 1999; Hernandez-Molina et al., 2006, 2008; Stow et al., 2009; Rebesco et al., 2014).

Relative to the smaller eastern moats, the larger western moats may record a faster flowing core, i.e., the core of the southward OPDW (Fig. 13). The smaller (narrower and shallower) moats along the eastern sides of the mounded drifts (Figs. 4, 5 and 7) indicate a weaker, northward geostrophic flow concentrated along the eastern side of the trough due to the influence of the Coriolis force. The higher reflection amplitude of the seafloor along the western side of MD-7 (Fig. 7) arises from larger acoustic impedance (the product of sound speed and water density) contrast. This suggests coarser (higher sound speed) sediment deposited by more vigorous currents along the western side of the trough relative to weaker currents along the eastern side. Numerical simulation revealed the occurrence of a faster, southward current and a slower, northward current in the OPDW depth range along the northern and middle

Luzon Trough (Jiang et al., 2020).

The weaker northward current may represent a counter-current of the OPDW (Fig. 13), similar to current and counter-current pairs observed from other passages (e.g., the Orkney, Bruce, and Discovery passages) (Garabato et al., 2002; Garcia et al., 2016). Within the Bruce Passage, for example, dense Weddell Sea Deep Water overflows from the Weddell Sea into the Scotia Sea (Garabato et al., 2002). Overflow includes a faster northward-flowing current and a slower southward-flowing current; they generate channels (Garcia et al., 2016) and furrows (Lobo et al., 2011) along both sides of the passage.

Following interpretations from similar localities (Faugères et al., 1999; Hernandez-Molina et al., 2008; Rebesco et al., 2014; Miramontes et al., 2019), the CDS-1 plastered drifts probably indicate the existence of relatively slow currents. Rebesco et al. (2014), for example, characterize plastered drifts as generally forming along gentle slopes swept by relatively low-velocity currents. The Luzon mooring observations reported in Zhao et al. (2016) confirm lower current velocities along the trough sidewalls relative to the trough center. The depths of CDS-1 plastered drifts (2500–3200 m water depth) fall within the depth range of the lower OPDW layer (Figs. 11 and 12), indicating that these drifts formed from the deeper, denser layer of overflow with only minor (or absent) deposition from the upper (mixing) layer of overflow (Fig. 13B; Legg et al., 2009).

In the two contourite channels (Figs. 5 and 9), truncated reflections and scarce to absent channel fill indicate erosive flow channels formed by the OPDW entering from

the North Pacific Ocean and cascading down to the Luzon Trough (Fig. 1A; Tian et al., 2006; Zhao et al., 2014). Faster OPDW flows (up to 30 cm/s) appear in these channels (Fig. 7; Zhao et al., 2014).

#### *Contourite depositional system 2 (CDS-2)*

The deeper contourite depositional system, CDS-2, includes the large sheeted drift SD-1 (3500–3700 m water depth) plus the two smaller, smoothly mounded drifts, MD-5 and MD-6 (3510–3600 m water depth), and their associated moats. All of these features occur within the deepest part of the Luzon Trough (Fig. 2).

We interpret this depositional system as tied to the bottom water mass underlying the overflow of Pacific Deep Water (OPDW) in the Luzon Trough. The lower boundary of the OPDW (Fig. 11) is estimated to be 50–120 m below the maximum velocity water depth according to the previous velocity observations along the trough (Zhao et al., 2014; Zhou et al., 2014; Ye et al., 2019). Hence, the bottom water in the trough is at water depth over ~3450 m, with a slower velocity (Figs. 11–13). The dense sluggish bottom water probably represents the remaining water of the OPDW—that is, the water that did not enter the South China Sea because of the obstacles of Outlet-1 and 2 and remained in the trough (Fig. 11). Formed at depths >3450 m, CDS-2 lies beneath the direct influence of the OPDW. Fine silt within the modern sheeted drift resembles that commonly found within abyssal plain environments (Rebesco et al., 2014), where it indicates sweeping of the seafloor by very slow bottom currents (Faugeres et al., 1999; Hernandez-Molina et al., 2008; Stow et al., 2009; Rebesco et al., 2014). These characteristics are consistent with the

560 sluggish bottom water in the Luzon Trough beneath the vigorous OPDW (Zhao et al.,  
561 2014) (Figs. 11–13), which flows in a southward direction (Zhao et al., 2014).

562 The deep, very smoothly mounded drifts (MD-5 and MD-6) and their associated  
563 moats along the eastern side of the northern trough floor indicate a weak and narrow  
564 northward current. This current may represent a counter-current of the southward  
565 flowing bottom water in the trough (Fig. 13A).

#### 567 5.2.2 Terraces and water mass interfaces

568 The two terraces, T-1 and T-2, occur at 2900–3400 m water depth along the  
569 western wall of the northern trough. This depth coincides with the interface between  
570 the OPDW and the underlying water mass (Fig. 11). The terraces likely represent  
571 sedimentary processes associated with vertical fluctuations of this interface (Fig. 13B).  
572 Water mass interface mechanisms have been proposed to explain terraces in other  
573 marine basins (Hernández-Molina et al., 2009, 2016, 2018; Preu et al., 2013; Rebesco  
574 et al., 2014). For a relatively deep interface (i.e., below terrace depth), the  
575 fast-flowing OPDW causes erosion of terraces (Fig. 6). When the interface becomes  
576 shallower, the sluggish BW enables deposition along the terraces (Fig. 13B). Mooring  
577 observations in the trough documented the seasonal and intraseasonal variations of the  
578 OPDW (Zhou et al., 2014; Zhao et al., 2016), including intensified, thicker, deeper,  
579 denser OPDW in late fall; and weakened, thinner, shallower, lighter OPDW in spring.  
580 These observations indicate significant vertical fluctuations of the OPDW base, which

correspond well with our interpretation of the terrace formation.

### *5.3 Conceptual implications of the overflow of Pacific Deep Water processes*

#### *5.3.1 Overflow behavior in confined settings*

Our study observations and interpretations elucidate sedimentary processes associated with the overflow of Pacific Deep Water (OPDW) in the deep confined trough. Three characteristics of the OPDW emerge as critically linked to sedimentary evidence, which could be considered and compared to other overflows in deep confined gateways in future studies in order to deepen our understanding of overflow processes.

First, OPDW does not always reach the gateway seabed. The appearance of the CDS-2 indicates the action of the sluggish bottom water overlain by the CDS-1-related vigorous overflow water. Other gateways typically show overflow waters that clearly traverse gateway bottoms. Examples include Mediterranean Outflow Water, which flows through the Strait of Gibraltar (Baringer and Price, 1997; Sanchez-Leal et al., 2017), and Faroe Bank Channel Overflow, through the Faroe Bank Channel (Mauritzen et al., 2005; Fer et al., 2010; Hansen et al., 2016). In this study, OPDW flows over the Bashi Sill between 2100 and 2450 m water depth, then descends to its equilibrium horizon (as determined by its density) of ~3450 m water depth, and finally enters the South China Sea at Outlet-1 and 2. The OPDW's maximum depth of descent (~1000 m) is therefore less than that of dense overflow



waters. Mediterranean Overflow Water descends 1200–1400 m after exiting the strait of Gibraltar (Baringer and Price, 1997; Sanchez-Leal et al., 2017), and the Faroe Bank Channel Overflow descends 2200 m (Hansen et al., 2016). OPDW may not reach the bottom of the northern Luzon Trough because the overflow lacks sufficient density to penetrate the deepest parts of the trough. The supposition of insufficient density, with a  $0.07\text{--}0.08\text{ kg/m}^3$  difference around Bashi sill, is supported by oceanographic observations of the potential density referenced to 2000 decibar (Fig. 1C. Zhou et al., 2018). Moreover, the seismic reflection data described here do not show distinct reflections arising from abrupt changes in acoustic impedance (the product of sound speed and water density) within the OPDW portion of the water column. These proxies for density interfaces fail to appear at either upper or lower boundaries of the OPDW, or within regions affected by its overflow (Fig. 10). In other areas with more energetic and denser water masses relative to ambient water, seismic reflection data clearly delineate water masses (Yamashita et al., 2011; Gorman et al., 2018).

The reason for the small density difference between the OPDW and the underlying water in the Luzon Trough may be related to the existence of the sills at the exit, i.e., Outlet-1 and 2 (Figs. 1A and 11). Only the OPDW shallower than the depth of Outlet-1 and 2 (both  $\sim 2850\text{ m}$ ) in the trough could easily enter the South China Sea (Fig. 11), while the deeper portion of the overflow would be retained in the trough. The presence of sills at the entrance and exit of the gateway could be a key difference between the OPDW and those overflows that encounter only one sill before reaching the open sea/ocean. The mechanisms generating such a minor overflow

624 density difference merit further study.

625       Second, the lower (denser) layer of OPDW dominates the development of  
626 contourite features along the gateway flow path with little or no contribution from the  
627 water mass's upper (mixing) layer. Overflow waters commonly consist of an upper  
628 mixing layer and a lower, denser layer (Legg et al., 2009). In the Luzon Trough, the  
629 CDS-1 components flow mainly between 2500 and 3400 m water depth, a range that  
630 overlaps that of the lower overflow layer (Fig. 13B). Contourite features do not  
631 appear at shallower depths. The OPDW dense layer controls the formation of  
632 overflow-associated, large-scale depositional and erosional contourite features within  
633 the trough, while the mixing layer apparently makes no contribution. A similar  
634 situation occurs with Mediterranean Overflow Water along the middle slope of the  
635 Gulf of Cadiz, where large erosional and depositional features form primarily due to  
636 the denser overflow layer (Baringer and Price, 1997; Llave et al., 2001; 2007;  
637 Hernandez-Molina et al., 2003; 2014; Roque et al., 2012; Sanchez-Leal et al., 2017).  
638 The steep topography swept by the OPDW upper layer may act as a non-depositional  
639 factor. However, the development of the plastered drifts on the steep wall of the  
640 Luzon Trough in the depth range of the OPDW lower layer, which is sometimes  
641 steeper than the wall where the OPDW upper layer sweeps (Fig. 13B), indicates that  
642 the steep topography could not be the decisive factor behind non-deposition and  
643 non-erosion. The key might lie in the behaviour of the overflow upper layer itself: its  
644 lower velocity and mixing/turbulence taking could hinder continuous large-scale  
645 deposition and erosion. Again, the mechanisms impeding deposition and erosion by

the overflow upper layer call for further study.

Third, the southward-flowing OPDW and its northward counter-current are responsible for the formation of drift-associated moats along both sides of the gateway. Our data suggest that the deeper and wider moats linked to the larger mounded drifts along the western side of the Luzon Trough may be a result of the more vigorous, southward OPDW. The shallower and narrower moats associated with the smaller mounded drifts along the eastern side (Figs. 2, 3, 4, 5, and 7) may result from the weaker northward current. Such a counter-current could generate moats and drifts even within a very narrow passage such as the 6 km wide C-1 corridor (Figs. 2–5). No observation of cross-trough variations in the along-trough flow has been reported for the main Luzon Trough, yet a numerical simulation revealed the presence of the counter-current in the northern and middle Luzon Trough (Jiang et al., 2020). The occurrence and behaviour of the OPDW counter-current urgently call for long-term, cross-trough observations of the Luzon Trough. The overflow counter-current contributing to the formation of contourite features is a phenomenon also observed in the Bruce Passage and adjacent Scan Basin in Antarctica (Garabato et al., 2002; Garcia et al., 2016). There, the overflow of Weddell Sea Deep Water and its counter-current flow have formed contourite channels and furrows (narrower and less incised than contourite channels) along both sides of the gateway (Lobo et al., 2011; Garcia et al., 2016). The mechanisms underlying the generation of such overflow counter-currents merit further study.

## 5.4 Regional implications of the overflow of Pacific Deep Water processes

### 5.4.1 Overflow-generated contourites as a record of regional tectonics

The three seismic units within CDS-1 (SU1 through SU3) show significant differences in terms of their seismic configurations and external morphologies that reflect variations in OPDW flow from the middle to late Miocene, when the trough formed.

The divergent basin-fill configuration of SU3 (Figs. 4–7) indicates uneven deposition in a generally high-energy deep-sea setting (Sangree and Widemier, 1977), i.e., turbidites as calibrated by IODP wells in the South China Sea oceanic basin (Yin et al., 2020) and other marginal seas (Pickering et al., 2013). Therefore, SU3 points to an absence of significant contourite activity and, by extension, weak or absent OPDW circulation at the bottom of the trough during its deposition. The apparently weak or absent OPDW circulation during the early depositional stage of the Luzon Trough may owe to a wider and deeper connection between the Pacific Ocean and the South China Sea (Hall, 2002). In addition, during the early development of the Luzon Strait, fewer volcanoes in the Luzon Arc (Yang et al., 1996; Chen et al., 2015; Huang et al., 2018) meant less of a bathymetric barrier to water exchange between the Pacific Ocean and the South China Sea.

The aggradational reflection configuration of the younger units, SU2 and SU1 (Figs. 4–7), indicates regional enhancement of OPDW circulation after the early

depositional stage of the trough. The enhanced mounded shape of SU2 through the top of SU1 within the main axis of the trough (Fig. 7); and significant moat formation further records a regional increase in OPDW velocity during the latest depositional stage of the trough. Gradual strengthening of OPDW circulation coincides with regional closure and shallowing of the Luzon Trough, as well as more volcanic activity in the area given the Taiwan orogeny in middle to late Miocene times (Yang et al., 1996; Huang et al., 2018).

Three of the four mounded drifts within the C-1 corridor (MD-1, MD-3, and MD-4) north of the trough show a higher degree of local mounding in SU2 than in SU1. This difference could indicate a slight decrease in overflow velocity through the C-1 corridor during trough evolution and SU1 development. The modern C-1 corridor (2590–2850 m water depth) occurs in the shallower part of the denser OPDW (2500–3450 m water depth), where the current velocity is lower than that observed for the deeper part (Figs. 7, 9, 10, 11; Zhao et al., 2014). The shallower water depth of C-1 may result from a more protracted period of uplift in the north relative to south, due to oblique collision (Huang et al., 2018). The irregular evolution of MD-1, MD-3, and MD-4 relative to the narrowing trough may therefore arise from greater shoaling to the north during the Taiwan orogeny.

#### *5.4.2 Influence of the overflow of Pacific Deep Water on the South China Sea margin*

The overflow of Pacific Deep Water (OPDW) enters the South China Sea basin

from the Luzon Trough mainly through Outlet-1 (2850 m water depth) (Fig. 2; Zhao et al., 2014; Ye et al., 2019). Numerical modelling of overflow transport (Zhao et al., 2014) indicates that the OPDW then flows counter-clockwise along the continental margin of the South China Sea.

Three lines of evidence suggest that the OPDW drives the circulation of the SDW and SBW in the South China Sea and thus helps form the two large-scale contourite depositional systems observed along the lower continental slope and abyssal plain just south of the South China shelf and Dongsha Islands (Fig. 13A; Yin et al., 2019). First, the SDW (1500–2000 m water depth) and SBW (>2000 m water depth) within the South China Sea roughly overlap with the OPDW depth range (2000–3450 m water depth) in the Luzon Trough. Second, the generally counter-clockwise circulation of the SDW and SBW (Qu et al., 2006; Tian et al., 2006) matches the direction of OPDW flow (Zhao et al., 2014). Third, the development of the Dongsha Islands contourite depositional systems (~1.1 Ma to present; Yin et al., 2019) coincides with the setting of enhancing OPDW circulation from the middle-late Miocene to present. Together, these lines of evidence indicate that the OPDW has been driving SDW and SBW circulation in the South China Sea since at least 1.1 Ma, when the OPDW became vigorous enough to significantly influence the marginal sea. Further assessment of this hypothesis will require additional research and regional data collection.

## 6. Conclusions

The overflow of Pacific Deep Water (OPDW) movement within the Luzon Trough gateway generated a contourite depositional system (CDS-1) along its southward flow path through the trough. This system includes erosional (channel and moat), depositional (drift), and mixed (terrace) contourite features along the bottom of the trough and its adjacent flanks. The lower, denser layer of the overflow, in conjunction with its weaker, northward-flowing counter-current, was primarily responsible for the formation of these features, including moats found along both sides of the mounded drifts. The upper (mixing) layer of the overflow does not appear to have generated any significant depositional or erosional contourite features. In parts of the Luzon Trough deeper than ~3450 m water depth, the OPDW does not reach the bottom because of thermohaline density constraints (i.e., the relatively low OPDW density). In those areas, the denser bottom water in the trough circulates weakly beneath the OPDW, thus generating a deeper contourite depositional system (CDS-2), where a sheet-like drift dominates deposition.

OPDW flow has gradually strengthened with the narrowing of the Luzon Trough due to the Taiwan orogeny. Shoaling in the northernmost trough may also weaken overflow locally. During the latest depositional stage, this more vigorous overflow has developed more prominent contourite features within the Luzon Trough while also promoting the formation of large contourite features along the lower slope and deeper areas of the adjacent South China Sea. Future drilling endeavors in the Luzon Trough are needed to obtain more precise age constraints regarding the OPDW's evolution.

This work demonstrates the importance of overflows and gateways in controlling the morphology and sedimentary evolution of deep marine sedimentary systems. Similar multidisciplinary research efforts could shed further light on the role of gateways in moderating geological, oceanographic, and paleoceanographic processes.

### **Acknowledgements**

This research was funded by the National Natural Science Foundation of China (grant 41976067), the National Program on Global Change and Air-Sea Interaction, State Oceanographic Association of China (grant GASI-GEOGE-05), the National Natural Science Foundation of China (grants 41706043 and 41830540), Scientific Research Fund of the Second Institute of Oceanography, MNR (grant JG2004), and a China Geological Survey project (grant DD20190222). This research was conducted within the framework of “The Drifters” Research Group of the Royal Holloway University of London (United Kingdom) and relates to projects CTM2012-39599-C03, CGL2016-80445-R, and CTM2016-75129-C3-1-R. We thank Michele Rebesco and Qiliang Sun for their review and contribution to improving the manuscript before submission.

### **References**

Baringer, M.O.N., Price, J.F., 1997. Mixing and spreading of the Mediterranean outflow. *Journal of physical oceanography* 27, 1654–1677.



- 774 Berggren, W.A., 1982. Role of Ocean Gateways in Climate change. En: Climate in  
775 Earth History. Studies in Geophysics, National Academic Press, 118–125 pp.
- 776 Brackenridge, R. E., Stow, D. A., Hernández-Molina, F. J., Jones, C., Mena, A., Alejo,  
777 I., Ducassou, E., Llave, E., Ercilla, G., Nombela, M. A., Perez-Arlucea, M.,  
778 Frances, G., 2018. Textural characteristics and facies of sand-rich contourite  
779 depositional systems. *Sedimentology* 65(7), 2223–2252.
- 780 Cai, Z., Gan, J., Liu, Z., Hui, C. R., Li, J., 2020. Progress on the formation dynamics  
781 of the layered circulation in the South China Sea. *Progress in Oceanography* 181,  
782 102246.
- 783 Catuneanu, O., Abreu, V., Bhattacharya, J., Blum, M., Dalrymple, R., Eriksson, P.,  
784 Fielding, C.R., Fisher, W., Galloway, W., Gibling, M., 2009. Towards the  
785 standardization of sequence stratigraphy. *Earth-Science Reviews* 92, 1–33.
- 786 Chen, W.-H., Huang, C.-Y., Lin, Y.-J., Zhao, Q., Yan, Y., Chen, D., Zhang, X., Lan, Q.,  
787 Yu, M., 2015. Depleted deep South China Sea  $\delta^{13}\text{C}$  paleoceanographic events in  
788 response to tectonic evolution in Taiwan–Luzon Strait since Middle Miocene.  
789 *Deep Sea Research Part II: Topical Studies in Oceanography* 122, 195–225.
- 790 Chen, W.S., Yeh, J.J., Syu, S.J., 2019. Late Cenozoic exhumation and erosion of the  
791 Taiwan orogenic belt: New insights from petrographic analysis of foreland basin  
792 sediments and thermochronological dating on the metamorphic orogenic wedge.  
793 *Tectonophysics*, 750, 56–69.
- 794 Clift, P.D., Schouten H., Draut A.E., 2003. A general model of arc-continent collision  
795 and subduction polarity reversal from Taiwan and the Irish Caledonides.

- 796 Geological Society, London, Special Publications, 219(1), 81–98.
- 797 Clift, P., Lee, G.H., Anh Duc, N., Barckhausen, U., Van Long, H., Zhen, S, 2008.
- 798 Seismic reflection evidence for a Dangerous Grounds miniplate: No extrusion
- 799 origin for the South China Sea. *Tectonics*, 27(3), TC3008.
- 800 de Weger, W., Hernández-Molina, F.J., Flecker, R., Sierro, F.J., Chiarella, D.,
- 801 Krijgsman, W., Manar, M.A., 2020. Late Miocene contourite channel system
- 802 reveals intermittent overflow behavior. *Geology*. In press.
- 803 Dummann, W., Steinig, S., Hofmann, P., Flögel, S., Osborne, A.H., Frank, M., Herrle,
- 804 J.O., Bretschneider, L., Sheward, R.M., Wagner, T., 2019. The impact of Early
- 805 Cretaceous gateway evolution on ocean circulation and organic carbon burial in
- 806 the emerging South Atlantic and Southern Ocean basins. *Earth and Planetary*
- 807 *Science Letters*, 115890.
- 808 Faugères, J.C., Stow, D.A.V., Imbert, P., Viana, A., 1999. Seismic features diagnostic
- 809 of contourite drifts. *Marine Geology* 162, 1–38.
- 810 Fer, I., Voet, G., Seim, K.S., Rudels, B., Latarius, K., 2010. Intense mixing of the
- 811 Faroe Bank Channel overflow. *Geophysical Research Letters* 37, L02604.
- 812 Garabato, A.C.N., McDonagh, E.L., Stevens, D.P., Heywood, K.J., Sanders, R., 2002.
- 813 On the export of Antarctic bottom water from the Weddell Sea. *Deep Sea*
- 814 *Research Part II: Topical Studies in Oceanography* 49, 4715–4742.
- 815 Garcia, M., Hernandez-Molina, F.J., Llave, E., Stow, D.A.V., Leon, R.,
- 816 Fernandez-Puga, M.C., del Rio, V.D., Somoza, L., 2009. Contourite erosive
- 817 features caused by the Mediterranean Outflow Water in the Gulf of Cadiz:

- 818 Quaternary tectonic and oceanographic implications. *Marine Geology* 257, 24–  
819 40.
- 820 García, M., Lobo, F.J., Maldonado, A., Hernández-Molina, F.J., Bohoyo, F., Pérez,  
821 L.F., 2016. High-resolution seismic stratigraphy and morphology of the Scan  
822 Basin contourite fan, southern Scotia Sea, Antarctica. *Marine Geology* 378, 361–  
823 373.
- 824 Gordon, A.L., Orsi, A.H., Muench, R., Huber, B.A., Zambianchi, E., Visbeck, M.,  
825 2009. Western Ross Sea continental slope gravity currents. *Deep Sea Research*  
826 Part II: Topical Studies in Oceanography 56, 796–817.
- 827 Gordon, A.L., Tessler, Z.D., Villanoy, C., 2011. Dual overflows into the deep Sulu Sea.  
828 *Geophysical Research Letters* 38, L18606.
- 829 Gordon, A.L., Zambianchi, E., Orsi, A., Visbeck, M., Giulivi, C.F., Whitworth III, T.,  
830 Spezie, G., 2004. Energetic plumes over the western Ross Sea continental slope.  
831 *Geophysical Research Letters* 31, L21302.
- 832 Gorman, A.R., Smillie, M.W., Cooper, J.K., Bowman, M.H., Vennell, R., Holbrook,  
833 W.S., Frew, R., 2018. Seismic characterization of oceanic water masses, water  
834 mass boundaries, and mesoscale eddies SE of New Zealand. *Journal of*  
835 *Geophysical Research: Oceans* 123, 1519–1532.
- 836 Hall R., 2002. Cenozoic geological and plate tectonic evolution of SE Asia and the SW  
837 Pacific: computer-based reconstructions, model and animations. *Journal of Asian*  
838 *Earth Sciences*, 20(4), 353–431.
- 839 Hansen, B., Larsen, H., Margretha, K., Hátún, H., Østerhus, S., 2016. A stable Faroe

- 840 Bank Channel overflow 1995–2015. *Ocean Science* 12, 1205–1220.
- 841 Hayes, D.E., Lewis, S.D., 1984. A geophysical study of the Manila Trench, Luzon,  
842 Philippines: 1. Crustal structure, gravity, and regional tectonic evolution. *Journal*  
843 *of Geophysical Research: Solid Earth* 89, 9171–9195.
- 844 Hernández-Molina, F.J., Larter, R.D., Maldonado, A., Rodríguez- Fernández, J., 2003.  
845 Pliocene and Quaternary stratigraphic evolution of the Pacific margin offshore of  
846 the Antarctic Peninsula offshore from Adelaide Island. 9th International  
847 Symposium on Antarctic Earth Science. Potsdam (Germany). 8–12, September,  
848 Abstracts Volume, pp. 153–154
- 849 Hernández-Molina, F.J., Bohoyo, F., Naveira Garabato, A., Galindo-Zaldívar, J., Lobo,  
850 F., Maldonado, A., Rodríguez-Fernández, J., Somoza, L., Stow, D., Vázquez, J.  
851 US Geological Survey The National Academies, 2007. The Scan Basin evolution:  
852 oceanographic consequences of the deep connection between the Weddell and  
853 Scotia Seas (Antarctica).
- 854 Hernández-Molina, F.J., Larter, R., Rebesco, M., Maldonado, A., 2006. Miocene  
855 reversal of bottom water flow along the Pacific Margin of the Antarctic  
856 Peninsula: stratigraphic evidence from a contourite sedimentary tail. *Marine*  
857 *Geology* 228, 93–116.
- 858 Hernández-Molina, F.J., Llave, E., Preu, B., Ercilla, G., Fontan, A., Bruno, M., Serra,  
859 N., Gomiz, J., Brackenridge, R., Sierro, F., 2014. Contourite processes associated  
860 with the Mediterranean Outflow Water after its exit from the Strait of Gibraltar:  
861 Global and conceptual implications. *Geology* 42, 227–230.

- 862 Hernández-Molina, F.J., Maldonado, A., Stow, D., 2008. Abyssal plain contourites.  
863 Developments in Sedimentology 60, 345–378.
- 864 Hernández-Molina, F.J., Campbell, S., Badalini, G., Thompson, P., Walker, R., Soto,  
865 M., Conti, B., Preu, B., Thieblemont, A., Hyslop, L., 2018. Large bedforms on  
866 contourite terraces: Sedimentary and conceptual implications. *Geology* 46, 27–  
867 30.
- 868 Hernández-Molina, F.J., Paterlini, M., Violante, R., Marshall, P., de Isasi, M., Somoza,  
869 L., Rebesco, M., 2009. Contourite depositional system on the Argentine Slope:  
870 an exceptional record of the influence of Antarctic water masses. *Geology* 37,  
871 507–510.
- 872 Hernández-Molina, F.J., Sierro, F.J., Llave, E., Roque, C., Stow, D.A.V., Williams, T.,  
873 Lofi, J., Van der Schee, M., Arnáiz, A., Ledesma, S., Rosales, C.,  
874 Rodríguez-Tovar, F.J., Pardo-Igúzquiza, E., Brackenridge, R.E., 2016. Evolution  
875 of the gulf of Cadiz margin and southwest Portugal contourite depositional  
876 system: Tectonic, sedimentary and paleoceanographic implications from IODP  
877 expedition 339. *Marine Geology* 377, 7–39.
- 878 Huang, C.-Y., Chen, W.-H., Wang, M.-H., Lin, C.-T., Yang, S., Li, X., Yu, M., Zhao,  
879 X., Yang, K.-M., Liu, C.-S., Hsieh, Y.-H., Harris, R., 2018. Juxtaposed sequence  
880 stratigraphy, temporal-spatial variations of sedimentation and development of  
881 modern-forming forearc Lichi Mélange in North Luzon Trough forearc basin  
882 onshore and offshore eastern Taiwan: An overview. *Earth-Science Reviews* 182,  
883 102–140.

- 884 Jiang, Y., Zhang, S., Tian, J., Zhang, Z., Gan, J., Wu, C. R., 2020. An Examination of  
 885 Circulation Characteristics in the Luzon Strait and the South China Sea Using  
 886 High-Resolution Regional Atmosphere-Ocean Coupled Models. *Journal of*  
 887 *Geophysical Research: Oceans* 125(6), e2020JC016253.
- 888 Jochumsen, K., Moritz, M., Nunes, N., Quadfasel, D., Larsen, K.M., Hansen, B.,  
 889 Valdimarsson, H., Jonsson, S., 2017. Revised transport estimates of the Denmark  
 890 Strait overflow. *Journal of Geophysical Research: Oceans* 122, 3434–3450.
- 891 Kaneko, I., Takatsuki, Y., Kamiya, H., 2001. Circulation of intermediate and deep  
 892 waters in the Philippine Sea. *Journal of oceanography* 57(4), 397–420.
- 893 Kennet, J.P., 1982. The geologic record of bottom currents. In: Kennet, J.P. (Ed.), *Marine*  
 894 *Geology*. Prentice Hall, Englewood Cliffs, New Jersey, pp. 505–534.
- 895 Knutz, P. C., Cartwright, J., 2003. Seismic stratigraphy of the West Shetland Drift:  
 896 Implications for late Neogene paleocirculation in the Faeroe-Shetland gateway.  
 897 *Paleoceanography* 18(4), 1093.
- 898 Knutz, P.C., 2008. Paleooceanographic significance of contourite drifts. In: Rebesco,  
 899 M., Camerlenghi, A. (Eds.), *Contourites*. Elsevier, Amsterdam, *Developments in*  
 900 *Sedimentology* 60, pp. 511–535.
- 901 Lee, T. Y., Tang, C. H., Ting, J. S., Hsu, Y. Y., 1993. Sequence stratigraphy of the  
 902 Tainan Basin, offshore southwestern Taiwan. *Petroleum Geology of Taiwan* 28,  
 903 119–158.
- 904 Legg, S., Briegleb, B., Chang, Y., Chassignet, E.P., Danabasoglu, G., Ezer, T., Gordon,  
 905 A.L., Griffies, S., Hallberg, R., Jackson, L., 2009. Improving oceanic overflow

- 906 representation in climate models: the gravity current entrainment climate process  
 907 team. *Bulletin of the American Meteorological Society* 90, 657–670.
- 908 Li, C.F., Xu, X., Lin, J., Sun, Z., Zhu, J., Yao, Y., Zhao, X., Liu, Q., Kulhanek, D.K.,  
 909 Wang, J., 2014. Ages and magnetic structures of the South China Sea constrained  
 910 by deep tow magnetic surveys and IODP Expedition 349. *Geochemistry,*  
 911 *Geophysics, Geosystems* 15, 4958–4983.
- 912 Lin, A.T., Watts, A.B., 2002. Origin of the West Taiwan basin by orogenic loading and  
 913 flexure of a rifted continental margin. *Journal of Geophysical Research: Solid*  
 914 *Earth* 107(B9): ETG 2-1–ETG 2-19.
- 915 Llave, E., Hernández-Molina, F.J., Somoza, L., Díaz-del-Río, V., Stow, D.A.V.,  
 916 Maestro, A., Alveirinho Dias, J.M., 2001. Seismic stacking pattern of the  
 917 Faro-Albufeira contourite system (Gulf of Cadiz): a Quaternary record of  
 918 paleoceanographic and tectonic influences. *Marine Geophysical Researches* 22,  
 919 487–508.
- 920 Llave, E., Hernández-Molina, F.J., Stow, D.A.V., Fernández-Puga, M.C., García, M.,  
 921 Vázquez, J.T., Maestro, A., Somoza, L., Díaz del Río, V., 2007. Reconstructions  
 922 of the Mediterranean Outflow Water during the quaternary based on the study of  
 923 changes in buried mounded drift stacking pattern in the Gulf of Cadiz. *Marine*  
 924 *Geophysical Research* 28, 379–394.
- 925 Lobo, F.J., Hernández-Molina, F.J., Bohoyo, F., Galindo-Zaldívar, J., Maldonado, A.,  
 926 Martos, Y., Rodríguez-Fernández, J., Somoza, L., Vázquez, J.T., 2011. Furrows  
 927 in the southern Scan Basin, Antarctica: interplay between tectonic and

- 928 oceanographic influences. *Geo-Marine Letters* 31, 451–464.
- 929 Maldonado, A., Barnolas, A., Bohoyo, F., Galindo-Zaldivar, J., Hernández-Molina, J.,  
 930 Lobo, F., Rodríguez- Fernández, J., Somoza, L., Vázquez, J.T., 2003. Contourite  
 931 deposits in the central Scotia Sea: the importance of the Antarctic Circumpolar  
 932 Current and the Weddell Gyre flows. *Palaeogeography, Palaeoclimatology,*  
 933 *Palaeoecology* 198, 187–221.
- 934 Mauritzen, C., Price, J., Sanford, T., Torres, D., 2005. Circulation and mixing in the  
 935 Faroese Channels. *Deep Sea Research Part I: Oceanographic Research Papers* 52,  
 936 883–913.
- 937 McCave, I., Lonsdale, P., Hollister, C., Gardner, W., 1980. Sediment transport over  
 938 the Hatton and Gardar contourite drifts. *Journal of Sedimentary Petrology* 50,  
 939 1049–1062.
- 940 McIntosh, K., (2014). Processed multichannel seismic data off Taiwan, acquired  
 941 during R/V Marcus G. Langseth expedition MGL0908 (2009) as part of the  
 942 Taiwan Integrated GEodynamics Research project (TAIGER). Integrated Earth  
 943 Data Applications (IEDA). doi:10.1594/IEDA/500026
- 944 McIntosh, K. D., Lavier, L., Lester, W. R., Eakin, D., Wu, F. T., Liu, C-S., Lee, C-S.,  
 945 2013a. Processed multichannel seismic data off Taiwan, acquired during R/V  
 946 Marcus G. Langseth expedition MGL0905 (2009) as part of the Taiwan  
 947 Integrated GEodynamics Research project (TAIGER). Academic Seismic Portal at  
 948 UTIG, Marine Geoscience Data System. Doi:10.1594/IEDA/500024
- 949 McIntosh, K. D., Lavier, L., Lester, W. R., Eakin, D., Wu, F. T., Liu, C-S., Lee, C-S.,



- 2013b. Processed multichannel seismic data off Taiwan, acquired during R/V  
 Marcus G. Langseth expedition MGL0906 (2009) as part of the Taiwan  
 Integrated GEodynamics Research project (TAIGER). Academic Seismic Portal at  
 UTIG, Marine Geoscience Data System. doi:10.1594/IEDA/500025
- Miramontes, E., Garreau, P., Caillaud, M., Jouet, G., Pellen, R., Hernández-Molina,  
 F.J., Clare, M.A., Cattaneo, A.J.G., 2019. Contourite distribution and bottom  
 currents in the NW Mediterranean Sea: Coupling seafloor geomorphology and  
 hydrodynamic modelling. *Geomorphology* 333, 43–60.
- Mitchum Jr, R., Vail, P., Sangree, J., 1977. Seismic stratigraphy and global changes of  
 sea level: Part 6. Stratigraphic interpretation of seismic reflection patterns in  
 depositional sequences: Section 2. Application of seismic reflection  
 configuration to stratigraphic interpretation.
- Nielsen T, Knutz P C, Kuijpers A., 2008. Seismic expression of contourite  
 depositional systems. In: Rebesco, M., Camerlenghi, A. (Eds.), *Contourites*.  
 Elsevier, Oxford, pp. 301–321.
- Pérez, L.F., Hernández-Molina, F.J., Lodolo, E., Bohoyo, F., Galindo-Zaldívar, J.,  
 Maldonado, A., 2019. Oceanographic and climatic consequences of the tectonic  
 evolution of the southern scotia sea basins, Antarctica. *Earth-Science Reviews*  
 198, 102922.
- Peters, H., Johns, W.E., 2005. Mixing and entrainment in the Red Sea outflow plume.  
 Part II: Turbulence characteristics. *Journal of Physical Oceanography* 35, 584–  
 600.

- Pickering, K. T., Underwood, M. B., Saito, S., Naruse, H., Kutterolf, S., Scudder, R., ... Slagle, A., 2013. Depositional architecture, provenance, and tectonic/eustatic modulation of Miocene submarine fans in the Shikoku Basin: Results from Nankai Trough Seismogenic Zone Experiment. *Geochemistry, Geophysics, Geosystems* 14(6), 1722–1739.
- Preu, B., Hernández-Molina, F.J., Violante, R., Piola, A.R., Paterlini, C.M., Schwenk, T., Voigt, I., Krastel, S., Spiess, V., 2013. Morphosedimentary and hydrographic features of the northern Argentine margin: the interplay between erosive, depositional and gravitational processes and its conceptual implications. *Deep Sea Research Part I: Oceanographic Research Papers* 75, 157–174.
- Qu, T., Song, Y. T., Yamagata, T., 2009. An introduction to the South China Sea throughflow: Its dynamics, variability, and application for climate. *Dynamics of Atmospheres and Oceans* 47(1-3), 3–14.
- Qu, T., Girton, J.B., Whitehead, J.A., 2006. Deepwater overflow through Luzon strait. *Journal of Geophysical Research: Oceans* 111, C01002.
- Qu, T., Mitsudera, H., Yamagata, T., 2000. Intrusion of the north Pacific waters into the South China Sea. *Journal of Geophysical Research: Oceans* 105(C3), 6415–6424.
- Qu, T., Mitsudera, H., Yamagata, T., 1999. A climatology of the circulation and water mass distribution near the Philippine coast. *Journal of Physical Oceanography* 29, 1488–1505.
- Rebesco, M., 2005. Contourites. In: Selley, R.C., Cocks, L.R.M., Plimer, I.R. (Eds.),

- 994 Encyclopedia of Geology. Elsevier, Oxford, pp. 513–527.
- 995 Rebesco, M., Camerlenghi, A., 2008. Contourites. Elsevier Science.
- 996 Rebesco, M., Hernández-Molina, F.J., Van Rooij, D., Wåhlin, A., 2014. Contourites  
997 and associated sediments controlled by deep-water circulation processes:  
998 State-of-the-art and future considerations. *Marine Geology* 352, 111–154.
- 999 Rebesco, M., Stow, D., 2001. Seismic expression of contourites and related deposits:  
1000 a preface. *Marine Geophysical Researches* 22, 303–308.
- 1001 Ricou LE., 1995. The Plate Tectonic History of the Past Tethys Ocean. In: Nairn  
1002 A.E.M., Ricou LE., Vrielynck B., Dercourt J. (Eds.) *The Tethys Ocean*.  
1003 Springer, Boston, MA, 3–70 pp.
- 1004 Roque, C., Duarte, H., Terrinha, P., Valadares, V., Noiva, J., Cachão, M., Ferreira, J.,  
1005 Legoinha, P., Zitellini, N., 2012. Pliocene and Quaternary depositional model of  
1006 the Algarve margin contourite drifts (Gulf of Cadiz, SW Iberia): Seismic  
1007 architecture, tectonic control and paleoceanographic insights. *Marine Geology*  
1008 303–306, 42–62.
- 1009 Sánchez-Leal, R.F., Bellanco, M.J., Fernández-Salas, L.M., García-Lafuente, J.,  
1010 Gasser-Rubinat, M., González-Pola, C., Hernández-Molina, F.J., Pelegrí, J.L.,  
1011 Peliz, A., Relvas, P., 2017. The Mediterranean Overflow in the Gulf of Cadiz: A  
1012 rugged journey. *Science advances* 3, eaao0609.
- 1013 Sangree, J., and Widmier, J., 1977. Seismic stratigraphy and global changes of sea  
1014 level, part 9: Seismic interpretation of clastic depositional facies: *AAPG Bulletin*  
1015 62, 752–771.

- 1016 Schlitzer, R., 2016. Ocean Data View. <http://odv.awi.de>.
- 1017 Schnuerle, P., Liu, C-S., Reed, D., Lundberg, N., McIntosh, K. D., Moore, G. F.,  
 1018 Nakamura, Y., Wu, F., T., 2008. Processed multichannel seismic data collected  
 1019 off Taiwan, acquired during the R/V Maurice Ewing survey EW9509 (1995).  
 1020 Academic Seismic Portal at UTIG, Marine Geoscience Data System.  
 1021 doi:10.1594/IEDA/500138
- 1022 Sibuet, J.C, Hsu, S.K., 2004. How was Taiwan created? *Tectonophysics*, 379(1-4),  
 1023 159–181.
- 1024 Sijp, W.P., von der Heydt, A.S., Dijkstra, H.A., Flögel, S., Douglas, P.M.J., Bijl, P.K.,  
 1025 2014, The role of ocean gateways on cooling climate on long time scales. *Global*  
 1026 *Plan. Change*, 119: 1–22.
- 1027 Stow, D.A.V., Hernández-Molina, F.J., Llave, E., Bruno, M., García, M., Díaz del Río,  
 1028 V., Somoza, L., Brackenridge, R.E., 2013. The Cadiz Contourite Channel: Sandy  
 1029 contourites, bedforms and dynamic current interaction. *Marine Geology* 343, 99–  
 1030 114.
- 1031 Stow, D. A., Hernández-Molina, F. J., Llave, E., Sayago-Gil, M., Díaz del Río, V.,  
 1032 Branson, A., 2009. Bedform-velocity matrix: the estimation of bottom current  
 1033 velocity from bedform observations. *Geology*, 37(4), 327–330.
- 1034 Stow, D., Smillie, Z., 2020. Distinguishing between Deep-Water Sediment Facies:  
 1035 Turbidites, Contourites and Hemipelagites. *Geosciences* 10(2), 68.
- 1036 Suppe, J., 1981. Mechanics of mountain building and metamorphism in Taiwan.  
 1037 *Memoir of the Geological Society of China* 4(6), 67–89.

- 1038 Taylor, B., Hayes, D.E., 1980. The tectonic evolution of the South China Basin.  
1039 Geophysical Monograph Series 23, 89–104.
- 1040 Teng, L.S., 1990. Geotectonic evolution of late Cenozoic arc-continent collision in  
1041 Taiwan. *Tectonophysics* 183(1-4), 57–76.
- 1042 Tian, J., Yang, Q., Liang, X., Xie, L., Hu, D., Wang, F., Qu, T., 2006. Observation of  
1043 Luzon Strait transport. *Geophysical Research Letters* 33, L19607.
- 1044 Yamashita, M., Yokota, K., Fukao, Y., Kodaira, S., Miura, S., Katsumata, K., 2011.  
1045 Seismic reflection imaging of a Warm Core Ring south of Hokkaido. *Exploration*  
1046 *Geophysics* 42, 18–24.
- 1047 Yang, K. M., Wu, J. C., Cheng, E. W., Chen, Y. R., Huang, W. C., Tsai, C. C., Wang, J.  
1048 T., Ting, H. H., 2014. Development of tectonostratigraphy in distal part of  
1049 foreland basin in southwestern Taiwan. *Journal of Asian Earth Sciences* 88, 98–  
1050 115.
- 1051 Yang, T.F., Lee, T., Chen, C.-H., Cheng, S.-N., Knittel, U., Punongbayan, R.S.,  
1052 Rasdas, A.R., 1996. A double island arc between Taiwan and Luzon:  
1053 consequence of ridge subduction. *Tectonophysics* 258, 85–101.
- 1054 Yaremchuk, M., McCreary Jr, J., Yu, Z., Furue, R., 2009. The South China Sea  
1055 throughflow retrieved from climatological data. *Journal of Physical*  
1056 *Oceanography* 39(3), 753–767.
- 1057 Ye, R., Zhou, C., Zhao, W., Tian, J., Yang, Q., Huang, X., Zhang, Z., Zhao, X., 2019.  
1058 Variability in the Deep Overflow through the Heng-Chun Ridge of the Luzon  
1059 Strait. *Journal of Physical Oceanography* 49, 811–825.

- 1060 Yin, S., Li, J., Ding, W., Sawyer, D. E., Wu, Z., Tang, Y., 2020. Sedimentary filling  
1061 characteristics of the South China Sea oceanic basin, with links to tectonic  
1062 activity during and after seafloor spreading. *International Geology Review*  
1063 62(7-8), 887–907.
- 1064 Yin, S., Hernández-Molina, F.J., Zhang, W., Li, J., Wang, L., Ding, W., Ding, W.,  
1065 2019. The influence of oceanographic processes on contourite features: A  
1066 multidisciplinary study of the northern South China Sea. *Marine Geology* 415,  
1067 105967.
- 1068 Zachos, J., Pagani, H., Sloan, L., Thomas, E. and Billups, K., 2001, Trends, rhythms,  
1069 and aberrations in global climate 65 Ma to present. *Science*, 292: 686–693.
- 1070 Zhang, Z., Zhao, W., Tian, J., Yang, Q., Qu, T., 2015. Spatial structure and temporal  
1071 variability of the zonal flow in the Luzon Strait. *Journal of Geophysical Research:*  
1072 *Oceans* 120, 759–776.
- 1073 Zhao, W., Zhou, C., Tian, J., Yang, Q., Wang, B., Xie, L., Qu, T., 2014. Deep water  
1074 circulation in the Luzon Strait. *Journal of Geophysical Research: Oceans* 119,  
1075 790–804.
- 1076 Zhao, X., Zhou, C., Zhao, W., Tian, J., Xu, X., 2016. Deepwater overflow observed by  
1077 three bottom-anchored moorings in the Bashi Channel. *Deep Sea Research Part I:*  
1078 *Oceanographic Research Papers* 110, 65–74.
- 1079 Zhou, C., Zhao, W., Tian, J., Yang, Q., Huang, X., Zhang, Z., Qu, T., 2018.  
1080 Observations of Deep Current at the Western Boundary of the Northern  
1081 Philippine Basin. *Scientific reports* 8, 14334.

- Zhou, C., Zhao, W., Tian, J., Yang, Q., Qu, T., 2014. Variability of the deep-water overflow in the Luzon Strait. *Journal of Physical Oceanography* 44, 2972–2986.
- Zhu, Y., Sun, J., Wang, Y., Li, S., Xu, T., Wei, Z., Qu, T., 2019. Overview of the multi-layer circulation in the South China Sea. *Progress in Oceanography*, 175, 171–182.

**Table-I.** General morphologic parameters of contourite features within the northern and middle Luzon Trough

Contourite features		Water depth (m)	Length (km)	Width (km)	Contourite depositional system		
Depositional	Drifts	MD-1	2780–2850	17	6	CDS-1	
		MD-2	2750–2800	17	2	CDS-1	
		MD-3	2600–2670	10	4	CDS-1	
		Mounded	MD-4	2590–2630	4	2	CDS-1
		MD-5	3510–3580	17	3	CDS-2	
		MD-6	3560–3600	8	5	CDS-2	
		MD-7	3200–3400	19	5	CDS-1	
	Plastered	PD-1	2500–2800	9	2	CDS-1	
		PD-2	2900–3200	8	3	CDS-1	
		PD-3	3000–3200	12	1	CDS-1	
	Sheeted	SD-1	3500–3700	220	25	CDS-2	
Channels		CC-1	2600–3000	110	2	CDS-1	
		CC-2	2650–2700	65	12	CDS-1	
		Moats		2700–3400	<=19	2	CDS-1
	3500–3700		<=17	2	CDS-2		
Mixed	Terraces	T-1	2900–3400	60	7	–	
		T-2	3000–3400	17	5	–	

## Figure captions

**Figure 1.** A) Regional bathymetric map of the northeastern South China Sea and northwestern Pacific Ocean, including regional ocean circulation patterns, sketch map of tectonics, and data collection locations for this study. The sizes of the blue arrows indicate the volume transport of the OPDW, marked by the number with unit Sv ( $1 \text{ Sv} = 1 \times 10^6 \text{ m}^3/\text{s}$ ) close to the arrow. G1 through G4 respectively represent samples GX118BC, GX128BC, GX133BC, and GX138BC. *In situ* hydrographic stations (BC1, LT1, LT2, WG2) in the trough are cited from Zhao et al. (2014). B) Mean hydrographic (salinity and temperature) section L1 with a width of 187 km across the northern Luzon



Strait. Thermohaline data were downloaded from the NOAA World Ocean Database 2013. This figure is elaborated using Ocean Data View (Schlitzer, R., 2016). The black profile at the bottom of each section shows seafloor topography. The arrows indicate flow direction of water masses. A ‘•’ symbol in the center of a circle indicates flow coming out of the page (i.e., southward, towards the reader). The white triangles at the section top mark the locations of the hydrographic casts in (B) and (D). C) Mean density profiles in the deep South China Sea (18°–20°N, 119°–121°E), Luzon Trough, and the Pacific (21°–23°N, 122°–124°E), modified from Zhao et al., 2014 and Zhou et al., 2014. D) Sectional (L2) view of the potential density ( $\sigma_2$ ) based on CTD casts along the Bashi Channel, modified from Zhou et al., 2018. The profile locations of (B) and (D) are shown in panel (A). *Abbreviations:* OPDW = Overflow of Pacific Deep Water. SSW = South China Sea Surface Water. SIW = South China Sea Intermediate Water. SDW = South China Sea Deep Water. SBW = South China Sea Bottom Water. NPTW = North Pacific Tropical Water. NPIW = North Pacific Intermediate Water. PDW = Pacific Deep Water. SCS = South China Sea. HR = Heng-chun Ridge. LA = Luzon Arc. LT = Luzon Trough. BS = Bashi Sill. MT = Manila Trench. TC = Taitung Canyon.

**Figure 2.** Swath multibeam bathymetric map (A) and regional morphosedimentary map (B) of the Luzon Trough interpreted from multibeam and seismic data, including the main contourite depositional and erosional features. The gray outlines mark the zero (present sea surface) contours. The white lines in A

show the locations of select interpreted seismic sections. The gray rectangles mark close-up of bathymetry in Fig. 3. The black dots mark the locations of surface samples. The yellow line represents the bathymetric profile location in Fig. 11. *Abbreviations:* BC = Bashi Channel. C-1 = Corridor 1. CC = contourite channel. MD = mounded drift. PD = plastered drift. SD = sheeted drift. T-1 and -2 = terraces 1 and 2. TC = Taitung Canyon. E1 through 3 = elevations 1 through 3. MTD = mass transport deposit.

**Figure 3.** Close-up of multibeam bathymetry in the north (A), east (Bashi Channel) (B), north to middle (C), and middle (D) sectors across the Luzon Trough. The white lines show the locations of select interpreted seismic profiles. The black dot marks the location of surface sample G2. The color bar in “A” is suitable for the rest of the figures (B, C and D).

**Figure 4.** Seismic reflection profile across the northern end of corridor C-1 of the northern Luzon Trough. The interpreted seismic units SU1–SU3, discontinuities H1 and H2, and the mounded drifts MD-1 and MD-2 with their associated moats are indicated. Current direction is indicated by the circles: a ‘•’ symbol in the center of a circle indicates flow coming out of the page (i.e., southward). An ‘×’ indicates a current flowing into the page (i.e., northward). TWT = two-way travel time. See Fig. 2 for profile location.

**Figure 5.** Seismic reflection profile across the southern end of corridor C-1 of the northern Luzon Trough showing the interpreted seismic units SU1–SU3, discontinuities H1 and H2, mounded drifts MD-3 and MD-4 (along with their

1158 associated moats), and contourite channel CC-1. See Fig. 2 for profile  
 1159 location.

1160 **Figure 6.** Seismic reflection profile across the main axis of the northern Luzon  
 1161 Trough, showing: the interpreted seismic units SU1–SU3; discontinuities H1  
 1162 and H2; the sheeted drift (SD); mounded drift MD-6 (and its associated moat);  
 1163 plastered drift PD-1; and terrace T-1. See Fig. 2 for profile location.

1164 **Figure 7.** Seismic reflection profile across the middle Luzon Trough (A) showing the  
 1165 interpreted seismic units SU1–SU3, discontinuities H1 and H2, mounded drift  
 1166 MD-7 (with associated moats), and plastered drifts PD-2 and PD-3. B) The  
 1167 along-trough current velocity at site LT2 (Zhao et al., 2014) near MD-7 is  
 1168 shown by the green line in the water column and indicates a southward  
 1169 direction. Note that depth in meters (red) is shown together with TWT (see  
 1170 text for further information). See Fig. 2 for profile location and Fig. 1A for the  
 1171 site location.

1172 **Figure 8.** A work site photo of surface sample GX118BC (G1) from the northern  
 1173 Luzon Trough showing fine-grained material on the modern seafloor.

1174 **Figure 9.** Seismic reflection profile across the Bashi Channel (A) showing contourite  
 1175 channel CC-2. B) The along-trough (downstream) current velocity at site BC1  
 1176 in Zhao et al. (2014) for CC-2 is shown by the green line in the water column.  
 1177 See Fig. 2 for profile location and Fig. 1A for site location.

1178 **Figure 10.** Seismic images across the Bashi Channel of the northern Luzon Trough (A)

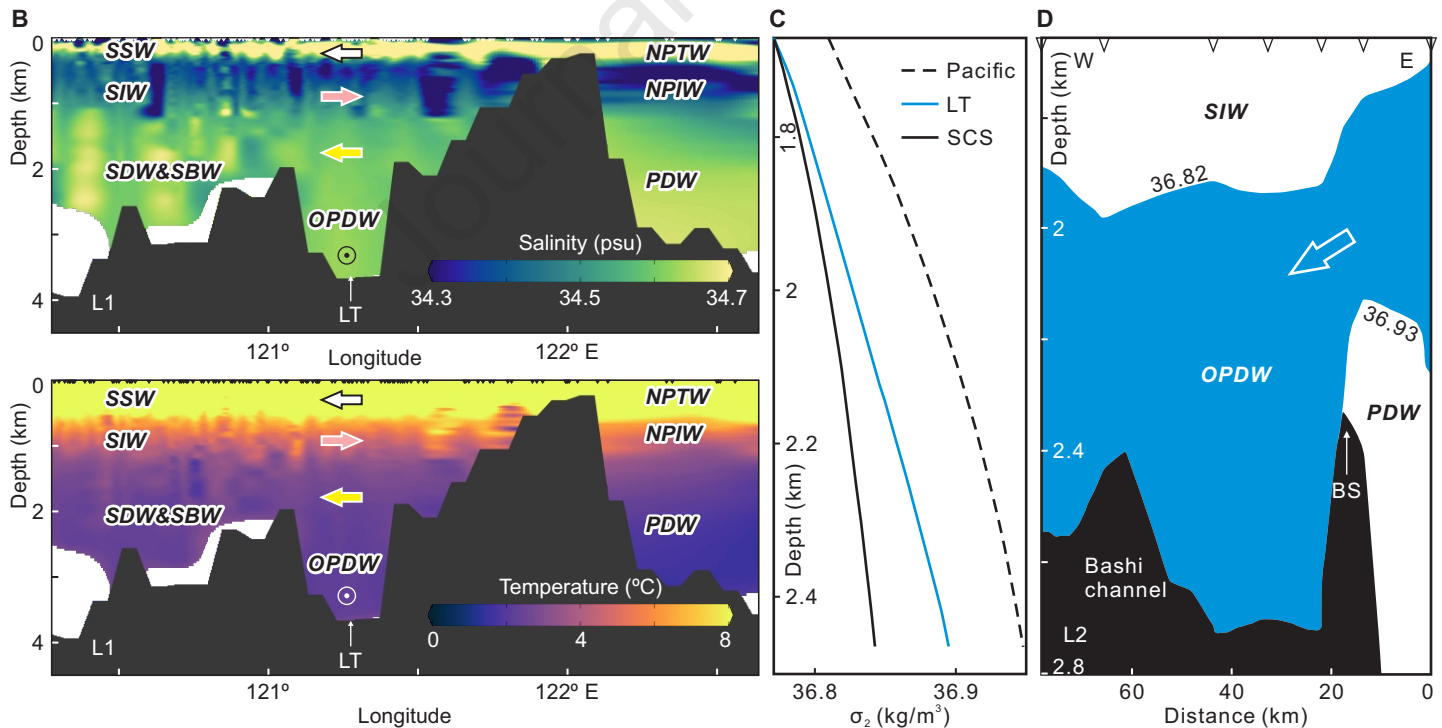
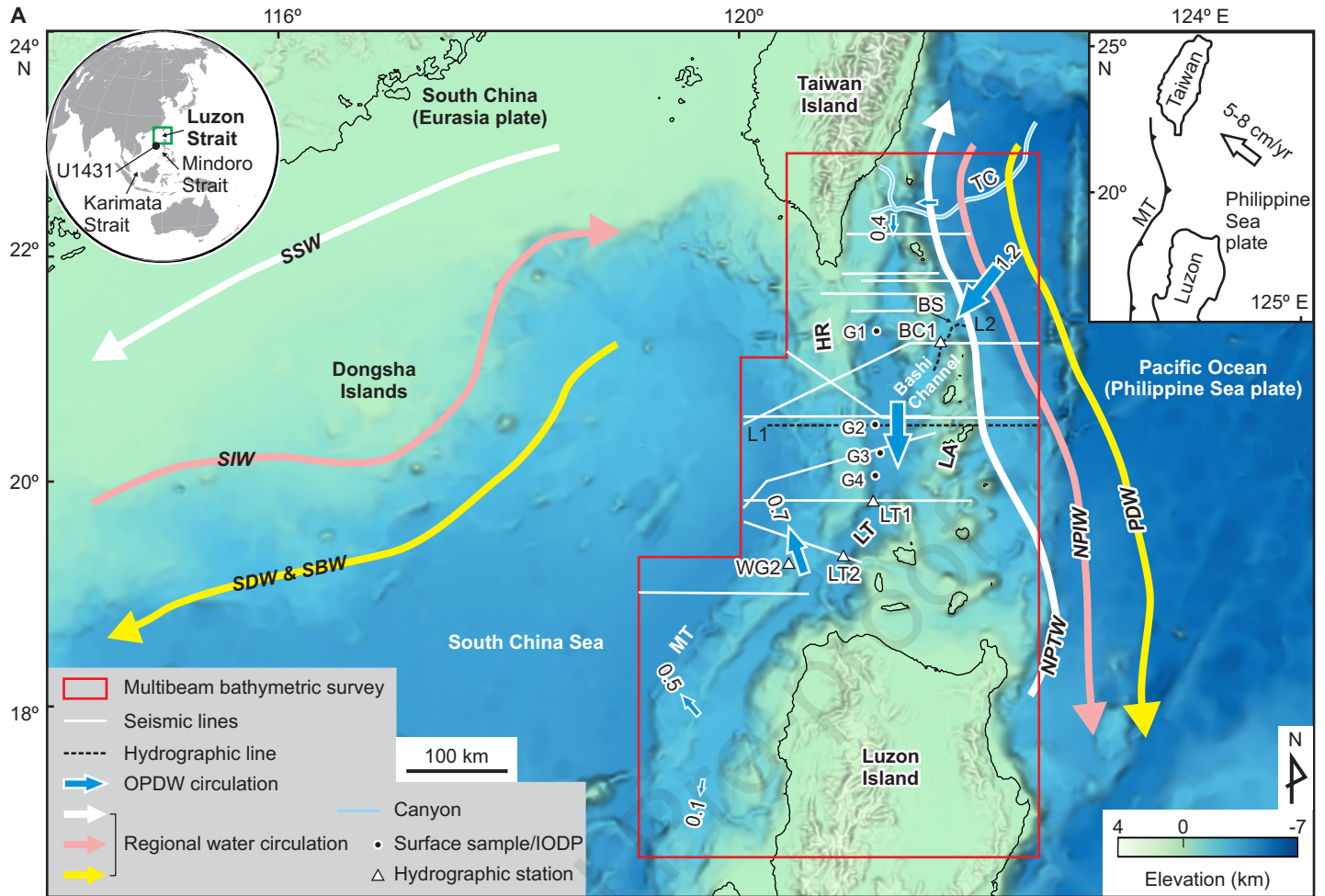
and across the southern trough (B), showing water masses and associated contourite features. Figure A shows contourite channel CC-2, and B shows mounded drift MD-3 along with plastered drifts PD-2 and PD-3. South China Sea Deep Water (SDW) is equivalent to Pacific Deep Water (PDW). The dashed lines mark the boundary of water masses. The vertical green lines show water-column profiles of nearby along-trough current velocities at sites BC1 and LT2 in Zhao et al. (2014). Positive values indicate southward, along-trough flow and negative values indicate northward, along-trough flow. See Fig. 2 for profile locations and Fig. 1A for site locations.

**Figure 11.** Mooring observations of current velocity along the Luzon Trough showing the general depth of the overflow of Pacific Deep Water (OPDW). Velocity profiles are adapted from Zhao et al. (2014). The black profile at the bottom shows seafloor topography. *Abbreviations:* BW = bottom water in the Luzon Trough. V = velocity. See Fig. 2 for the bathymetric profile location.

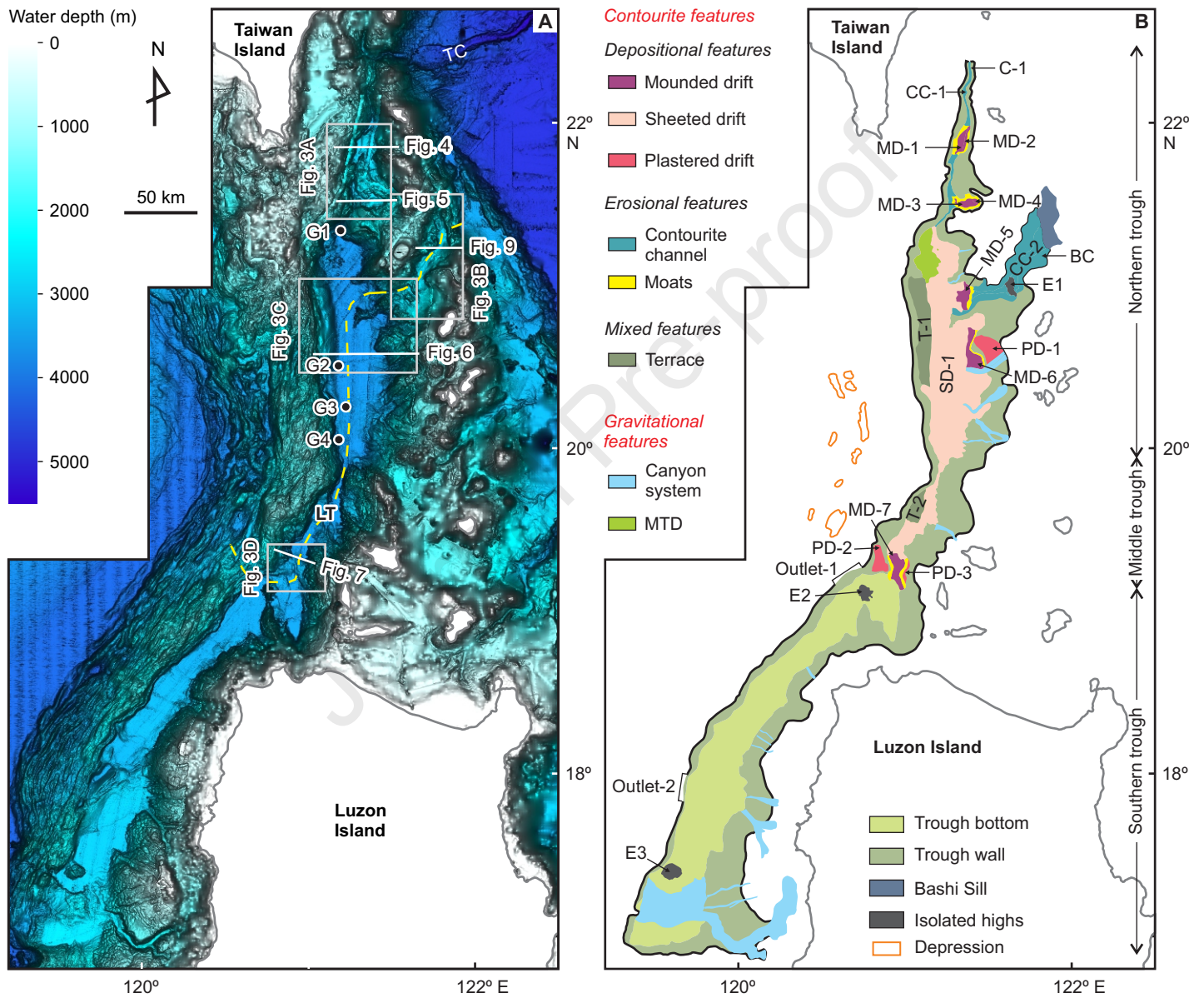
**Figure 12.** Seismic and vertical hydrographic (salinity and temperature) sections across the C-1 corridor (A, B) and the main course of the northern Luzon Trough (C, D). South China Sea Deep Water (SDW) is equivalent to Pacific Deep Water (PDW). The white dashed lines represent upper and lower boundaries of the overflow of Pacific Deep Water (OPDW). The white triangles at the sea surface mark the locations of the hydrographic casts. See Fig. 2 for section locations.

**Figure 13.** A) Sketch of the Luzon Trough (from entryways to Outlet-1), with the two

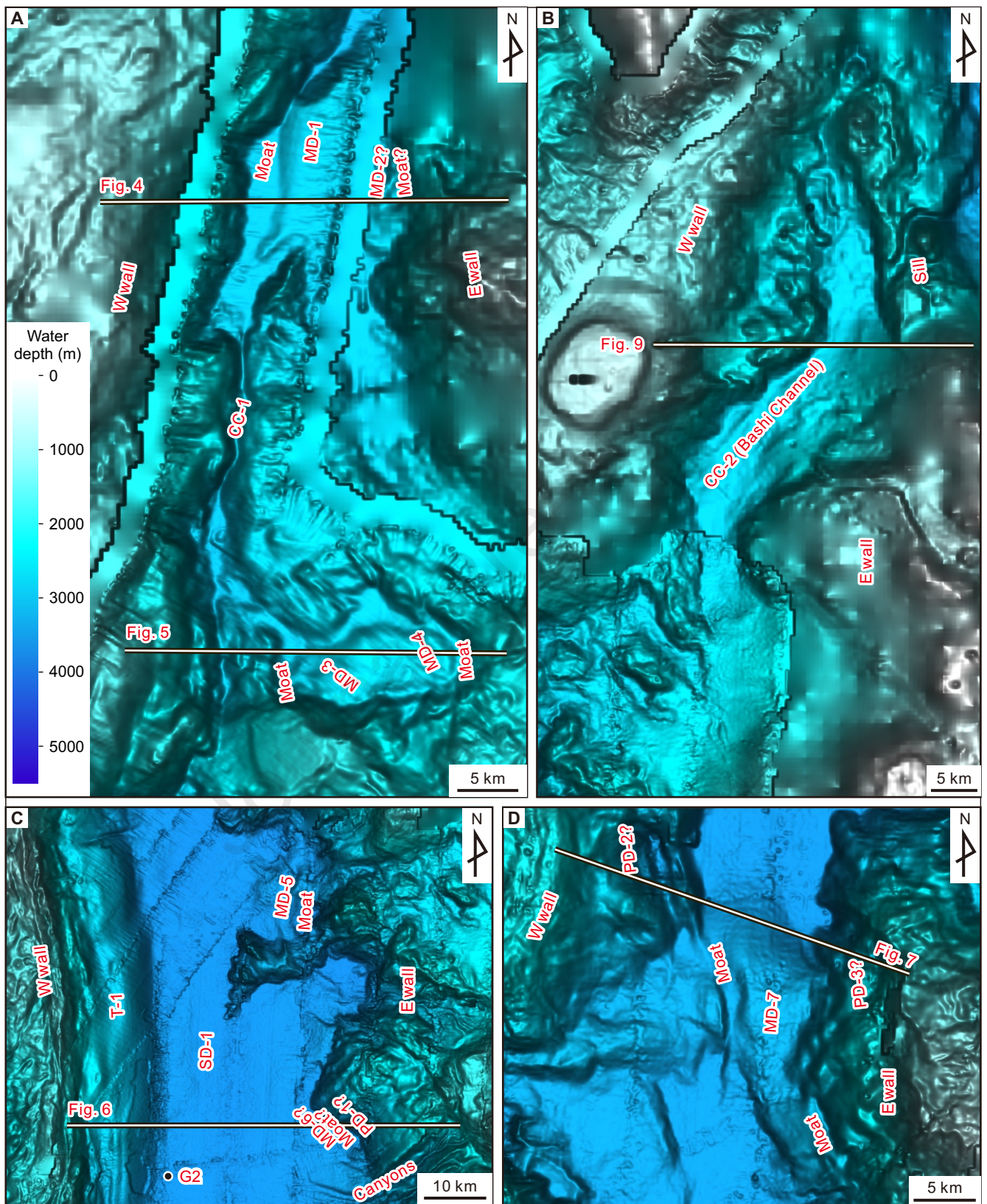
contourite depositional systems, CDS-1 and CDS-2. The thick black lines indicate the spatial boundary of the Luzon Trough, and the gray lines indicate outlines of major regional morphologic features. The solid blue arrows show the overflow of Pacific Deep Water (OPDW), and the open blue arrows show counter-current flow. Arrow size indicates relative transport volume. See Fig. 2B for the contourite features within and around the Luzon Trough. B) Vertical sections across the northern trough (section S1) and the middle trough (section S2) showing water masses and associated contourite features. The dashed line marks the possible shallower interface between the OPDW and bottom water in the Luzon Trough (BW) when the OPDW weakens. Section locations are shown in panel (A) by the dashed black lines. In the Luzon Trough, the OPDW controlled development of CDS-1, and the South China Sea Deep Water (SDW) controlled development of CDS-2.



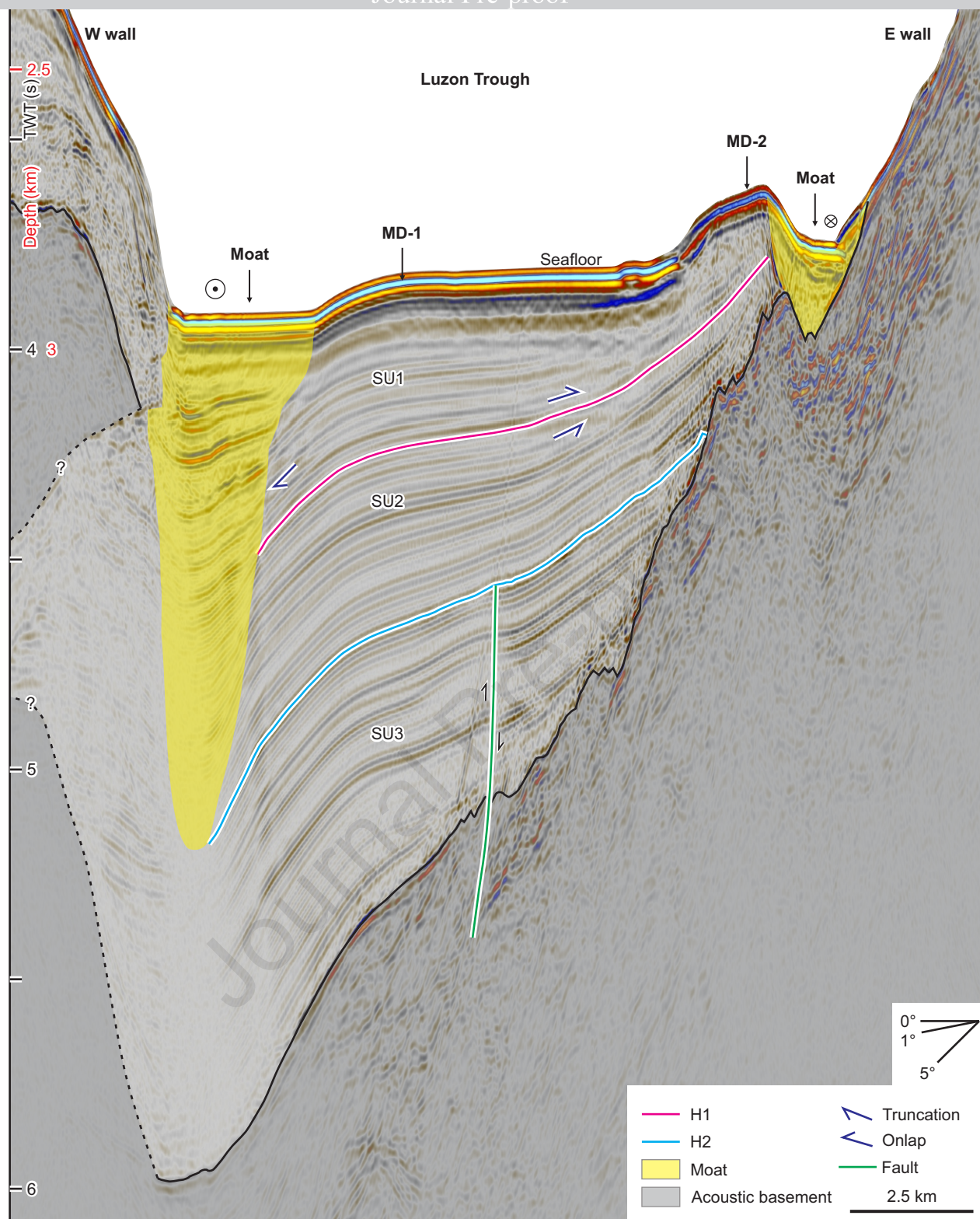




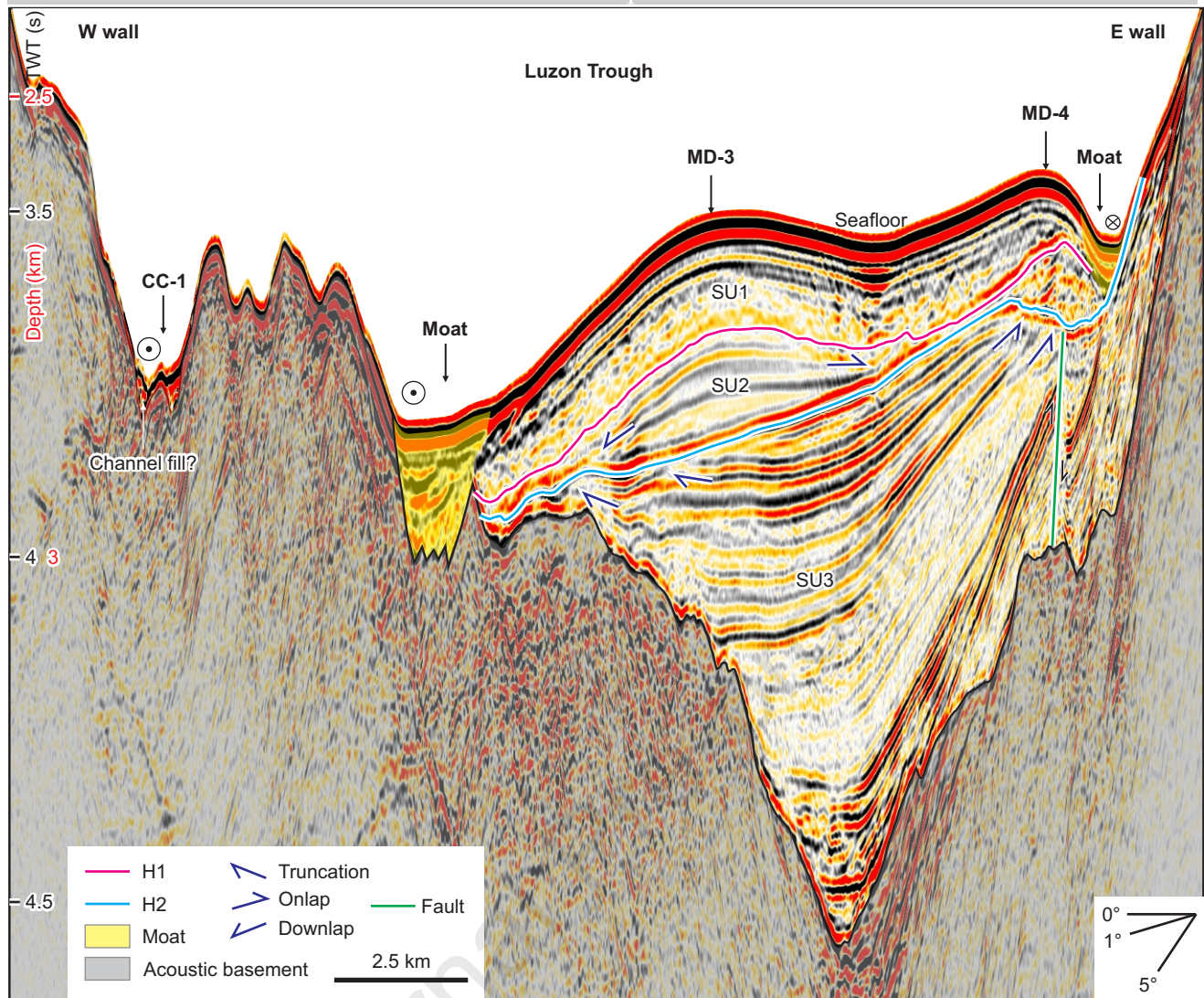




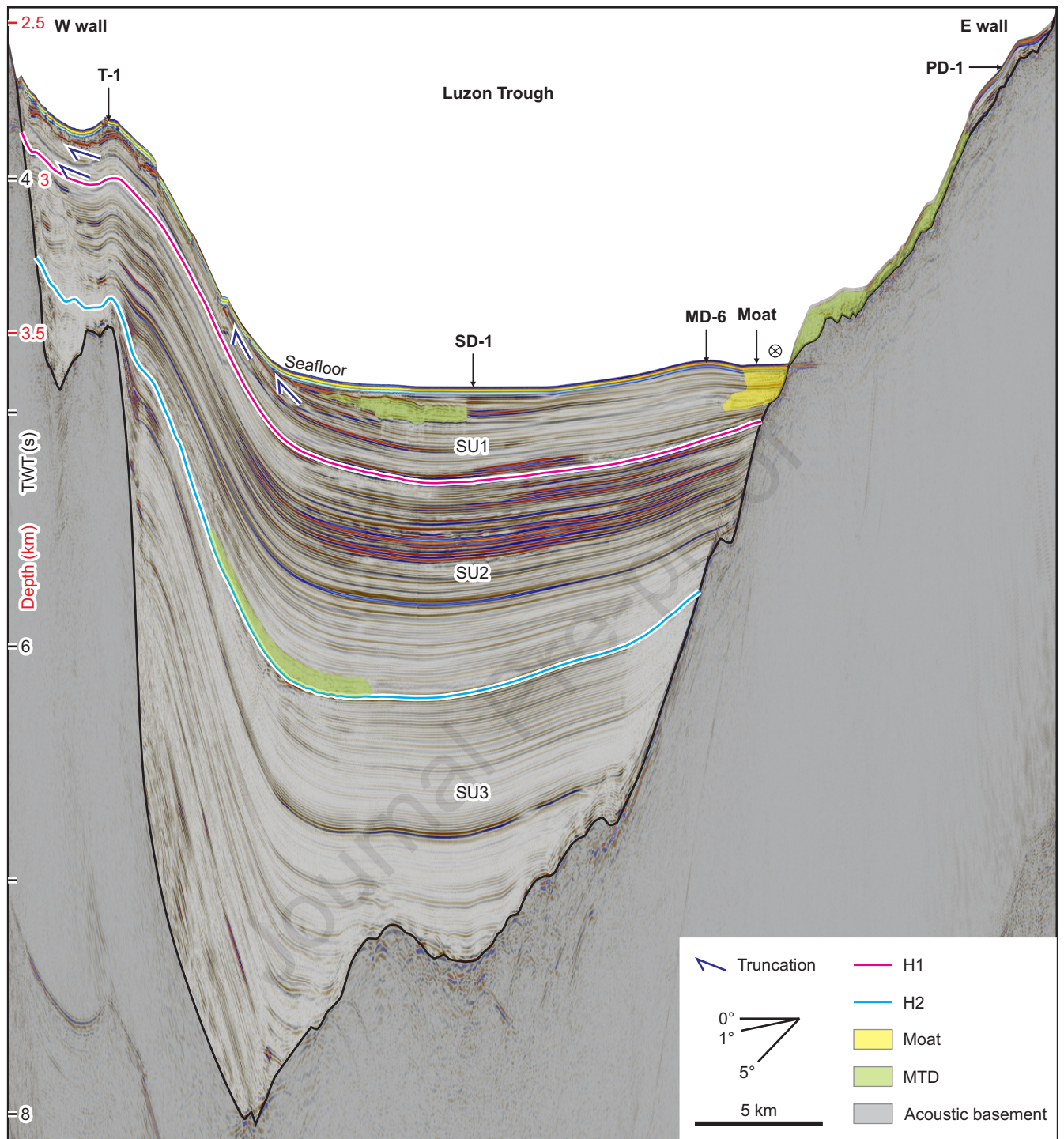




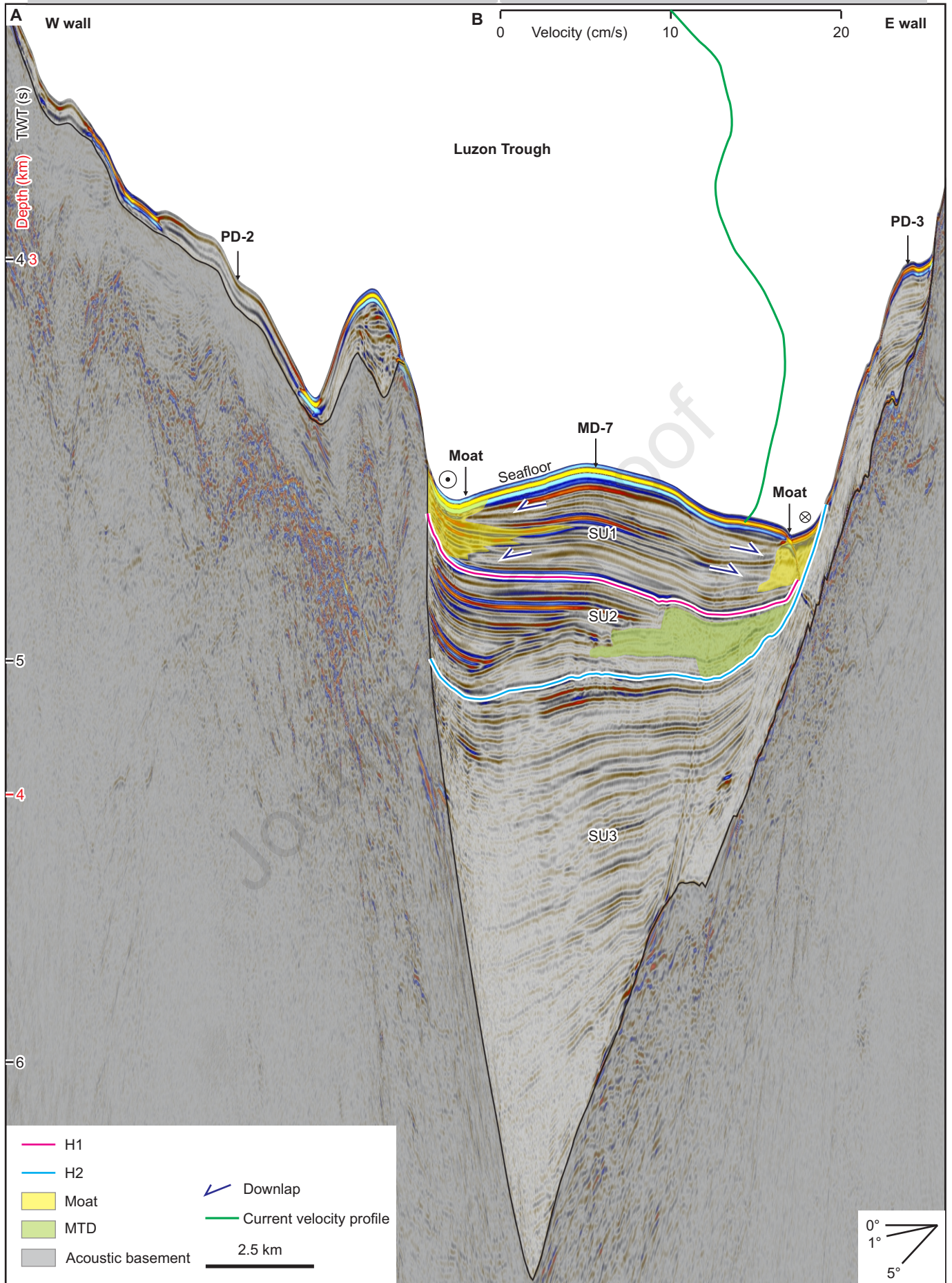


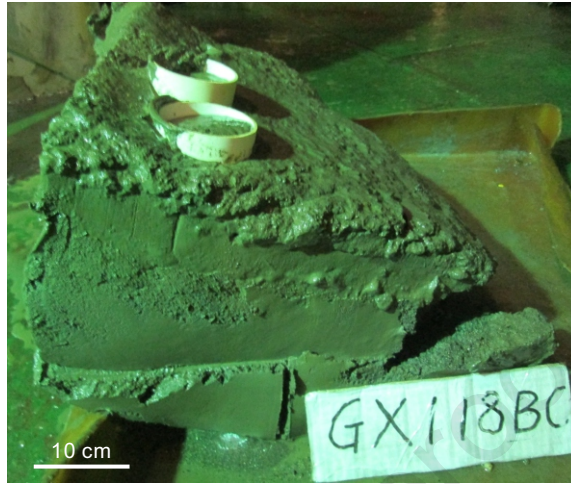




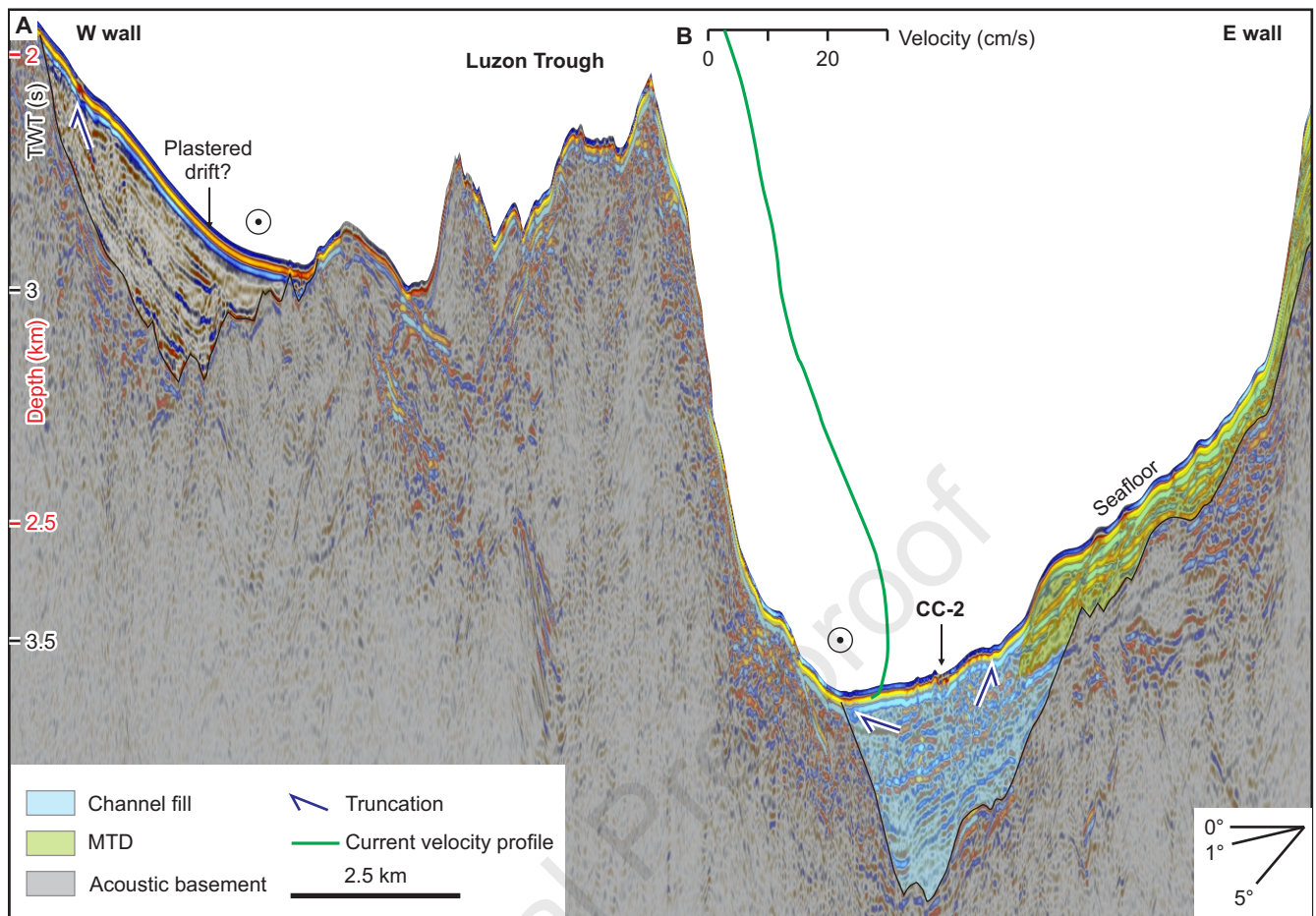


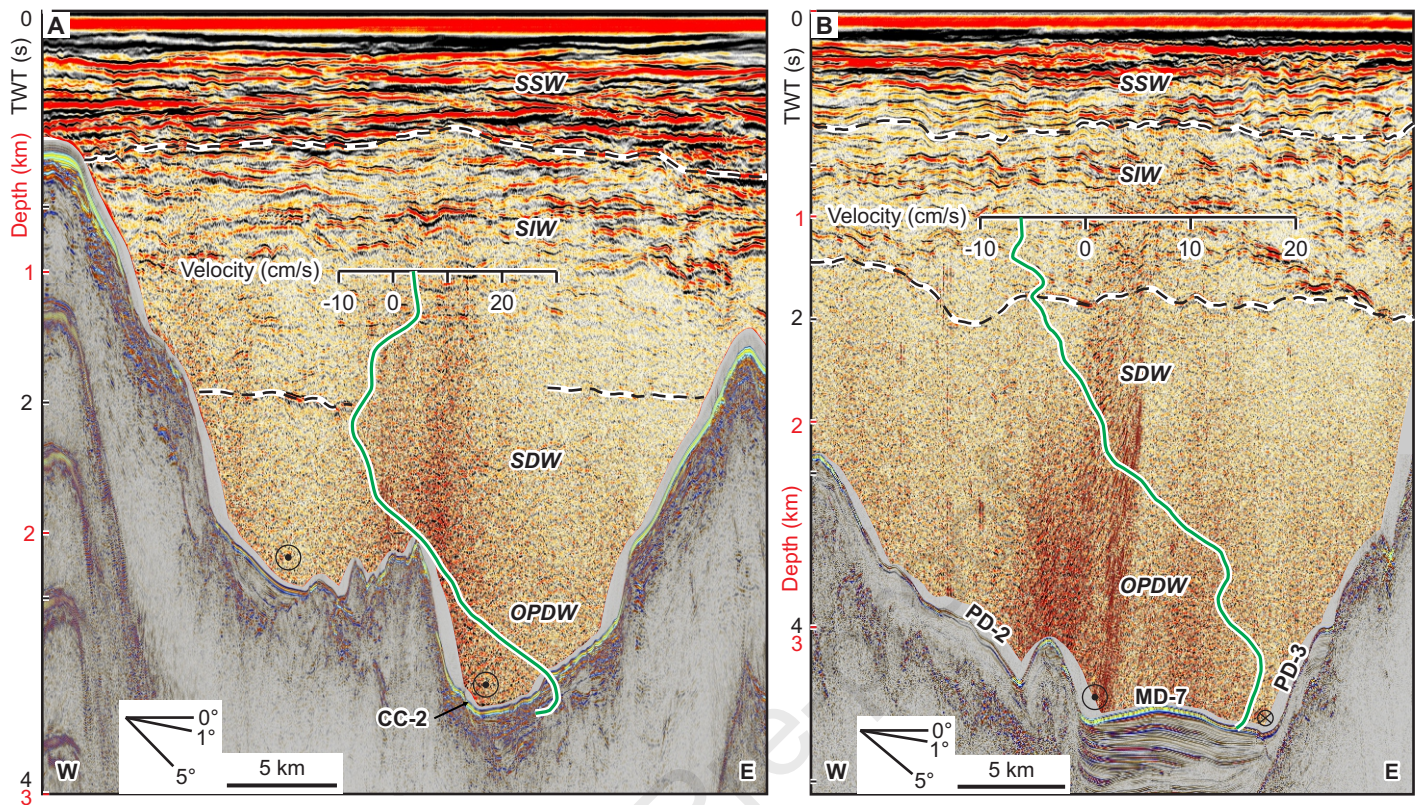


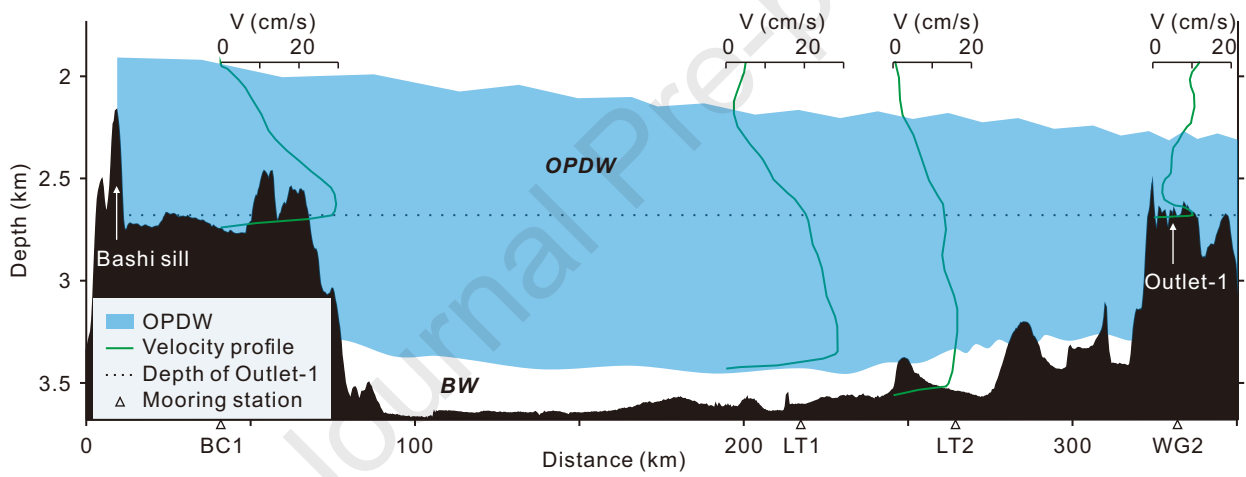




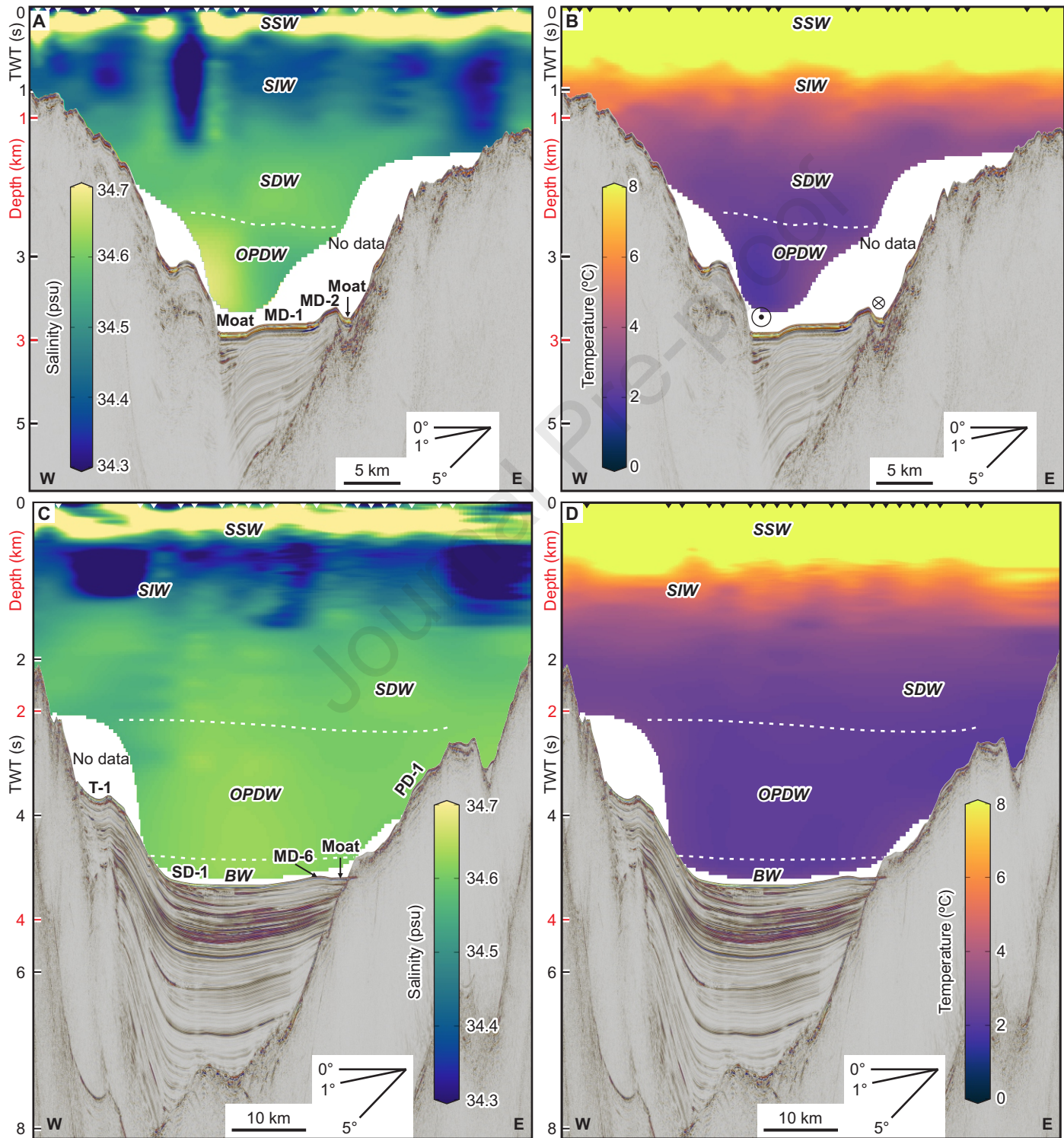


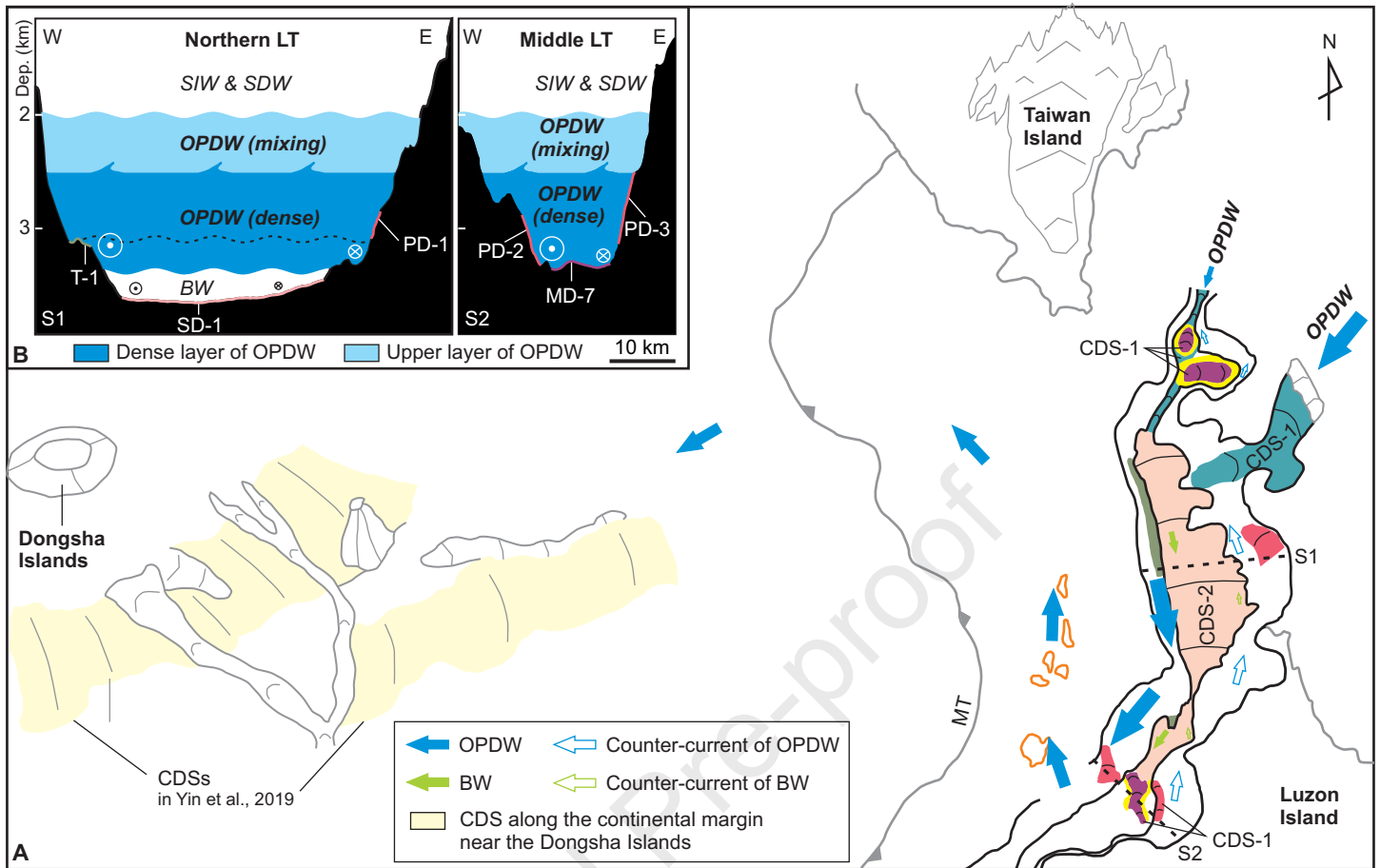












### **Highlights**

- Multidisciplinary study of the overflow of Pacific Deep Water along the Luzon Trough
- The overflow overlies a more sluggish layer at depth greater than 3450 m
- The overflow lower layer has formed a contourite depositional system
- The upper (mixing) layer of the overflow has not generated significant contourite features
- Gateway and overflow have influenced South China Sea morphology and sedimentary evolution

**Declaration of interests**

☒ The authors declare that they have no known competing financial interests or personal relationships that could have appeared to influence the work reported in this paper.

☐ The authors declare the following financial interests/personal relationships which may be considered as potential competing interests: